

A domain decomposition strategy for natural imposition of mixed boundary conditions in port-Hamiltonian systems

Sjoerd D.M. de Jong¹, Andrea Brugnoli², Ramy Rashad³, Yi Zhang⁴, and Stefano Stramigioli⁵

¹Department of Microelectronics, Delft University of Technology, Delft, Netherlands

²ICA, Université de Toulouse, ISAE–SUPAERO, INSA, CNRS, MINES ALBI, UPS, Toulouse, France

³Control and Instrumentation Engineering Department, King Fahd University of Petroleum and Minerals, Saudi Arabia

⁴School of Mathematics and Computing Science, Guilin University of Electronic Technology, Guilin, China

⁵Robotics and Mechatronics Department, University of Twente, The Netherlands

Abstract

[Abstract] In this contribution, a finite element scheme to impose mixed boundary conditions without introducing Lagrange multipliers is presented for wave propagation phenomena described as port-Hamiltonian systems. The strategy relies on finite element exterior calculus and a domain decomposition to interconnect two systems with different causalities. The spatial domain is split into two parts by introducing an arbitrary interface. Each subdomain is discretized with a mixed finite element formulation that introduces a uniform boundary condition in a natural way as the input. In each subdomain the spaces are selected from a finite element subcomplex to obtain a stable discretization. The two systems are then interconnected together by making use of a feedback interconnection. This is achieved by discretizing the boundary inputs using appropriate spaces that couple the two formulations. The final systems includes all boundary conditions explicitly and does not contain any Lagrange multiplier. Each subdomain is integrated using an implicit midpoint scheme in an uncoupled way from the other by means of a leapfrog scheme. The proposed strategy is tested on three different examples: the Euler-Bernoulli beam, the wave equation and the Maxwell equations. Numerical tests assess the conservation properties of the scheme and the effectiveness of the methodology.

1 Introduction

To simulate, design and analyze modern engineering technologies, modular modeling tools are of great importance, as they allow to simplify validation and verification, speed up prototyping and encapsulate complexity. Paradigms based on a modular description of systems are implemented in many widespread libraries like SIMULINK¹ or DIMOLA². In many cases, a reliable description of a complex technological devices is achieved by using coupled systems of partial differential equations (PDE) where different physics operate together. In recent years, the port-Hamiltonian (pH) formalism [1] has established itself as a sound and powerful mathematical framework for modeling and control of complex multiphysical systems. At the core of this framework lies the idea of composability, i.e. the fact that interconnecting together port-Hamiltonian systems (pHs) leads another system of the same kind.

¹<https://www.mathworks.com/products/simulink.html>

²<https://www.3ds.com/products/catia/dymola>

The theory of port-Hamiltonian systems is built upon a rich geometrical structure based on exterior calculus and issues may arise if this structure is not preserved at the numerical level, leading to spurious numerical solutions [2, 3, 4]. Structure preserving techniques attempt to capture as much of the underlying structures as possible. Many different structure preserving discretizations have been proposed throughout the years, such as mimetic finite differences [5, 6], discrete exterior calculus [7], finite element exterior calculus [3] and many others. When devising discretization schemes for port-Hamiltonian systems, boundary conditions have a prominent role in the discussion. This is due to the connection of port-Hamiltonian systems to the concept of Stokes-Dirac structure [8]. This geometrical structure characterizes all admissible boundary flows into a spatial domain and is agnostic to the causality of actual boundary conditions of the problem. The way boundary conditions are included in the model is related to the numerical method used. In a finite element context, boundary conditions are either imposed strongly by incorporating them in the discrete spaces used to approximate the variables or weakly when there are explicitly part of the weak formulation [9]. Weak imposition of the boundary conditions typically arises from the variational formulation in a natural manner via integration by parts. There is no general consensus on whether it is preferable to use a weak or strong formulation and the best choice is strongly problem and method dependent [10, 11]. Strong imposition of the boundary conditions in dynamical systems leads to differential-algebraic equations that are more difficult to solve than ordinary differential equations [12]. In the port-Hamiltonian community a general effort has been made to incorporate mixed boundary conditions in an explicit manner, see for instance [13] for a discrete exterior calculus formulation, [14] for a Galerkin scheme based on Whitney forms, [15] for a mixed finite element framework and [16] for discontinuous Galerkin discretization based on finite element exterior calculus (FEEC). Wave propagation phenomena exhibit a primal dual structure that was first highlighted in [17]. Therein however no connection with differential geometry is established. In [18] the authors used a finite element exterior calculus to highlight the fundamental primal-dual structure of pHs. The two formations are related by the Hodge operator and the resulting scheme is called dual-field as each variable is represented in dual finite element bases. The use of a dual field finite element formulation has been initially introduced in [19] as a way of handling the convective non-linearity of Navier-Stokes equations in an explicit manner and still obtaining a conservative scheme in terms of mass, helicity and energy. The work of [19] focused on periodic domains only without dealing with boundary conditions. In port-Hamiltonian systems, the dual field representation allows obtaining the topological power balance that characterizes the Dirac structure when inhomogeneous mixed boundary conditions are considered. Furthermore, it clearly shows that the two formulations have opposite causality of the boundary conditions, which leads to the question of how can this primal-dual structure be exploited for incorporating them.

In the present contribution, the dual-field representation is employed to achieve weak imposition of mixed boundary conditions in wave propagation phenomena. The spatial domain is decomposed using an internal interface that separates the two boundary subpartitions when a single boundary condition applies. On each subdomain a mixed finite element formulation is used in a such a way that the boundary condition is included naturally. Each mixed formulation uses a pair a finite elements that constitute an Hilbert subcomplex and thus is stable and structure preserving. The two formulations are then interconnected together on the shared interface by means of a feedback (or in port-Hamiltonian jargon a gyrator interconnection) that enforces in weak manner the continuity of the finite element spaces. The resulting system incorporates the mixed boundary conditions of the problem in a completely weak manner and does not require Lagrange multipliers. Even if the methodology is detailed for hyperbolic port-Hamiltonian systems, it can be extended to static elliptic problems. For the time integration the implicit midpoint scheme is used in each subdomain. The two coupling of the two is treated in an explicit manner by considering a time staggering of the two system via a Störmer Verlet method. This choice guarantees the preservation of the power balance in each subdomain [20]. The proposed approach will be shown to be accurate, have proper convergence and to be able to preserve certain mathematical, and thereby physical, properties at the discrete level. To demonstrate this, three different physical examples are considered: the Euler-Bernoulli beam in one dimension, then the wave

equation in two dimensions, and lastly the Maxwell equations in three dimensions. The examples chosen showcase the versatility of our approach in different physical-domains as well as different dimensions.

The outline of the rest of the paper is as follows, the assumptions of the study and the mixed discretization approach based on finite element subcomplexes is presented in Sec. 2. The domain-decomposition strategy and time-integration scheme is presented in Sec.3 including the choice of the finite element basis for the boundary input made to couple the two formulation on the interface. Section 4 presents the numerical validation of our scheme and finally we conclude the paper in Sec. 5.

2 Mixed Galerkin discretization of port-Hamiltonian systems

In this section the general class of port-Hamiltonian systems is presented. Then we recall the mixed finite element Galerkin discretization presented in [17]. This discretization is such to retain the Hamiltonian structure at the discrete level.

2.1 Linear port-Hamiltonian hyperbolic systems

Consider a domain $\Omega \subset \mathbb{R}^d$, $d \in \{1, 2, 3\}$ and a partition of its boundary $\partial\Omega = \bar{\Gamma}_1 \cup \bar{\Gamma}_2$, such that $\Gamma_1 \cap \Gamma_2 = \emptyset$. Let $\mathbf{x} = \{\boldsymbol{\alpha}, \boldsymbol{\beta}\}$ be the state variables. The states at a given time are expected to be square integrable functions $\boldsymbol{\alpha}(t) \in L^2(\Omega; \mathbb{A})$, $\boldsymbol{\beta}(t) \in L^2(\Omega; \mathbb{B})$ taking values in the vector spaces \mathbb{A} , \mathbb{B} .

To define the dynamics of the system, an unbounded differential operator $\mathcal{L} : L^2(\Omega; \mathbb{A}) \rightarrow L^2(\Omega; \mathbb{B})$ is introduced. For a given differential it is possible to define its formal adjoint by means of the integration by parts formula.

Definition 1 (Formal Adjoint) *Let $\mathbf{u} \in C_0^\infty(\Omega, \mathbb{A})$ and $\mathbf{v} \in C_0^\infty(\Omega, \mathbb{B})$ smooth variables on Ω , and \mathcal{L} be the differential operator $\mathcal{L} : L^2(\Omega; \mathbb{A}) \rightarrow L^2(\Omega; \mathbb{B})$. The formal adjoint of \mathcal{L} is than $\mathcal{L}^* : L^2(\Omega; \mathbb{B}) \rightarrow L^2(\Omega; \mathbb{A})$ defined by the relation*

$$(\mathcal{L}\mathbf{u}, \mathbf{v})_\Omega = (\mathbf{u}, \mathcal{L}^*\mathbf{v})_\Omega. \quad (1)$$

where the inner product of two functions is denoted by $(f, g)_\Omega = \int_\Omega f \cdot g \, d\Omega$.

The differential operator \mathcal{L} and its formal adjoint \mathcal{L}^* give rise to the Hilbert spaces $H^\mathcal{L}$ and $H^{\mathcal{L}^*}$, which are specified as

$$\begin{aligned} H^\mathcal{L}(\Omega) &= \{\mathbf{u} \in L^2(\Omega, \mathbb{A}) \mid \mathcal{L}\mathbf{u} \in L^2(\Omega, \mathbb{B})\}, \\ H^{\mathcal{L}^*}(\Omega) &= \{\mathbf{v} \in L^2(\Omega; \mathbb{B}) \mid \mathcal{L}^*\mathbf{v} \in L^2(\Omega; \mathbb{A})\}. \end{aligned} \quad (2)$$

The formal adjoint definition does not account for boundary terms arising from the integration by parts formula. They are introduced by means of the next assumption.

Assumption 1 (Abstract integration by parts) *Let $\mathbf{e}_\alpha \in H^\mathcal{L}(\Omega)$, $\mathbf{e}_\beta \in H^{\mathcal{L}^*}(\Omega)$. Then the following integration by parts formula is assumed to hold*

$$(\mathcal{L}\mathbf{e}_\alpha, \mathbf{e}_\beta)_\Omega = (\mathbf{e}_\alpha, \mathcal{L}^*\mathbf{e}_\beta)_\Omega + \langle \mathcal{T}_\alpha \mathbf{e}_\alpha, \mathcal{T}_\beta \mathbf{e}_\beta \rangle_{\partial\Omega}, \quad (3)$$

for appropriate trace operators, where $\langle f, g \rangle_{\partial\Omega} = \int_{\partial\Omega} f \cdot g \, d\Gamma$ denotes the inner product over the boundary.

Example 1 (Gradient and divergence operators) *Let $\mathcal{L} := \text{grad}$ be the gradient and $\mathcal{L}^* = -\text{div}$ be the negative of the divergence. Let $f \in H^1(\Omega)$, $\mathbf{v} \in H^{\text{div}}(\Omega)$ be a scalar and a vector function. The integration by parts states that the inner product with the gradient can be written as*

$$(\text{grad } f, \mathbf{v})_\Omega = -(f, \text{div } \mathbf{v})_\Omega + \langle f, \mathbf{v} \cdot \mathbf{n} \rangle_{\partial\Omega}. \quad (4)$$

In this case the trace operators correspond to the Dirichlet trace and the normal trace.

In this work we focus on conservation laws describing wave propagation phenomena in Hamiltonian form

$$\begin{pmatrix} \partial_t \boldsymbol{\alpha} \\ \partial_t \boldsymbol{\beta} \end{pmatrix} = \begin{bmatrix} 0 & -\mathcal{L}^* \\ \mathcal{L} & 0 \end{bmatrix} \begin{pmatrix} \delta_{\boldsymbol{\alpha}} H \\ \delta_{\boldsymbol{\beta}} H \end{pmatrix}. \quad (5)$$

where H is the Hamiltonian and $\delta_{\boldsymbol{\alpha}} H, \delta_{\boldsymbol{\beta}} H$ its variational derivative with respect to the state variables. In this work we restrict our attention to linear wave propagation phenomena described by the Hamiltonian formalism. The linearity of the system translates into a quadratic Hamiltonian.

Assumption 2 (Quadratic Hamiltonian) *The Hamiltonian is assumed to be quadratic in the state variable*

$$H = \frac{1}{2}(\boldsymbol{\alpha}, \mathcal{Q}_{\alpha} \boldsymbol{\alpha})_{\Omega} + \frac{1}{2}(\boldsymbol{\beta}, \mathcal{Q}_{\beta} \boldsymbol{\beta})_{\Omega}, \quad (6)$$

The operators \mathcal{Q}_{α} and \mathcal{Q}_{β} are symmetric and positive (and therefore invertible).

The variational derivative of the Hamiltonian (also called co-energy variables) are evaluated as follows [21]

$$\mathbf{e}_{\alpha} := \frac{\delta H}{\delta \boldsymbol{\alpha}} = \mathcal{Q}_{\alpha} \boldsymbol{\alpha}, \quad \mathbf{e}_{\beta} := \frac{\delta H}{\delta \boldsymbol{\beta}} = \mathcal{Q}_{\beta} \boldsymbol{\beta}. \quad (7)$$

Given (7), the state variables are related to the co-energy variables by

$$\boldsymbol{\alpha} = \mathcal{M}_{\alpha} \mathbf{e}_{\alpha}, \quad \boldsymbol{\beta} = \mathcal{M}_{\beta} \mathbf{e}_{\beta},$$

where $\mathcal{M}_{\alpha} := \mathcal{Q}_{\alpha}^{-1}$, $\mathcal{M}_{\beta} := \mathcal{Q}_{\beta}^{-1}$. The Hamiltonian 6 can be expressed in terms of co-energy variables as

$$H = \frac{1}{2}(\mathbf{e}_{\alpha}, \mathcal{M}_{\alpha} \mathbf{e}_{\alpha})_{\Omega} + \frac{1}{2}(\mathbf{e}_{\beta}, \mathcal{M}_{\beta} \mathbf{e}_{\beta})_{\Omega}. \quad (8)$$

The system can be equivalently rewritten in terms of the coenergy variables including mixed boundary conditions as follows

$$\begin{aligned} \begin{bmatrix} \mathcal{M}_{\alpha} & 0 \\ 0 & \mathcal{M}_{\beta} \end{bmatrix} \begin{pmatrix} \partial_t \mathbf{e}_{\alpha} \\ \partial_t \mathbf{e}_{\beta} \end{pmatrix} &= \begin{bmatrix} 0 & -\mathcal{L}^* \\ \mathcal{L} & 0 \end{bmatrix} \begin{pmatrix} \mathbf{e}_{\alpha} \\ \mathbf{e}_{\beta} \end{pmatrix}, & \mathbf{e}_{\alpha} \in H^{\mathcal{L}}(\Omega), \\ & & \mathbf{e}_{\beta} \in H^{\mathcal{L}^*}(\Omega), \\ \begin{pmatrix} \mathbf{u}_{\partial,1} \\ \mathbf{u}_{\partial,2} \end{pmatrix} &= \begin{bmatrix} \mathcal{T}_{\alpha}|_{\Gamma_1} & 0 \\ 0 & \mathcal{T}_{\beta}|_{\Gamma_2} \end{bmatrix} \begin{pmatrix} \mathbf{e}_{\alpha} \\ \mathbf{e}_{\beta} \end{pmatrix}, \\ \begin{pmatrix} \mathbf{y}_{\partial,1} \\ \mathbf{y}_{\partial,2} \end{pmatrix} &= \begin{bmatrix} 0 & \mathcal{T}_{\beta}|_{\Gamma_1} \\ \mathcal{T}_{\alpha}|_{\Gamma_2} & 0 \end{bmatrix} \begin{pmatrix} \mathbf{e}_{\alpha} \\ \mathbf{e}_{\beta} \end{pmatrix}, \end{aligned} \quad (9)$$

where $\mathbf{u}_{\partial,i}$, $i = \{1,2\}$ are the boundary conditions data. The notation $\mathcal{T}_{\alpha}|_{\Gamma_i}$, $\mathcal{T}_{\beta}|_{\Gamma_i}$, $i = \{1,2\}$ denotes the restriction of the trace operators to a given subpartition of the boundary. As customary in port-Hamiltonian system theory, the formulation includes collocated boundary outputs. The time derivative of the Hamiltonian gives

$$\dot{H} = \langle \mathbf{u}_{\partial,1}, \mathbf{y}_{\partial,1} \rangle_{\Gamma_1} + \langle \mathbf{u}_{\partial,2}, \mathbf{y}_{\partial,2} \rangle_{\Gamma_2}.$$

Remark 1 (Equivalence with Lagrangian dynamics) *The presented Hamiltonian formulation can be deduced from the a least action principle and is equivalent to a Lagrangian formulation [22].*

2.2 Mixed finite element discretization of port-Hamiltonian systems under uniform boundary conditions

The discretization of problem 9 is detailed in [17], where its primal-dual structure is highlighted. Therein however the point of view of Hilbert complexes is not considered and this mathematical structure is important for port-Hamiltonian system. In this section we will formulate the mixed problem and consider a finite element that respects the Hilbert complex structure. Furthermore, we detail the different numerical treatment of input and output variables.

The weak formulation can now be obtained by applying the test function $\mathbf{v} = \{\mathbf{v}_\alpha, \mathbf{v}_\beta\}$ and integrating over Ω to end up with

$$\begin{aligned} (\mathbf{v}_\alpha, \mathcal{M}_\alpha \partial_t \mathbf{e}_\alpha)_\Omega &= -(\mathbf{v}_\alpha, \mathcal{L}^* \mathbf{e}_\beta)_\Omega, \\ (\mathbf{v}_\beta, \mathcal{M}_\beta \partial_t \mathbf{e}_\beta)_\Omega &= (\mathbf{v}_\beta, \mathcal{L} \mathbf{e}_\alpha)_\Omega. \end{aligned} \quad (10)$$

Given the abstract integration by parts formula (3) two possibilities arise. One can either integrate by parts the first line or the second. Depending on the choice, two dynamical systems with opposite boundary causality are obtained. The choice is guided by the given boundary condition as one formulation will include the input $\mathbf{u}_{\partial,1}$, while the other includes $\mathbf{u}_{\partial,2}$. To illustrate this point, the discretization for the limiting case of uniform boundary conditions is considered next.

System 1: weak formulation for the case $\Gamma_1 = \partial\Omega$ If the second line is integrated by parts, the weak formulation reads: find $\mathbf{e}_{\alpha,1} \in L^2(\Omega; \mathbb{A})$ and $\mathbf{e}_{\beta,1} \in H^{\mathcal{L}^*}(\Omega)$ such that

$$\begin{aligned} (\mathbf{v}_{\alpha,1}, \mathcal{M}_\alpha \partial_t \mathbf{e}_{\alpha,1})_\Omega &= -(\mathbf{v}_{\alpha,1}, \mathcal{L}^* \mathbf{e}_{\beta,1})_\Omega, & \text{for all } \mathbf{v}_{\alpha,1} \in L^2(\Omega; \mathbb{A}), \\ (\mathbf{v}_{\beta,1}, \mathcal{M}_\beta \partial_t \mathbf{e}_{\beta,1})_\Omega &= (\mathcal{L}^* \mathbf{v}_{\beta,1}, \mathbf{e}_{\alpha,1})_\Omega + \langle \mathcal{T}_\beta \mathbf{v}_{\beta,1}, \mathbf{u}_{\partial,1} \rangle_{\partial\Omega}, & \text{for all } \mathbf{v}_{\beta,1} \in H^{\mathcal{L}^*}(\Omega), \\ \mathbf{y}_{\partial,1} &= \mathcal{T}_\beta|_{\partial\Omega} \mathbf{e}_{\beta,1}. \end{aligned} \quad (11)$$

The output is not evaluated weakly, but taken to be the trace of the associated state variable.

System 2: weak formulation for the case $\Gamma_2 = \partial\Omega$ If the first line is integrated by parts, the following system is obtained: find $\mathbf{e}_\alpha \in H^{\mathcal{L}}(\Omega)$, $\mathbf{e}_\beta \in L^2(\Omega; \mathbb{B})$ such that

$$\begin{aligned} (\mathbf{v}_{\alpha,2}, \mathcal{M}_\alpha \partial_t \mathbf{e}_{\alpha,2})_\Omega &= -(\mathcal{L} \mathbf{v}_{\alpha,2}, \mathbf{e}_{\beta,2})_\Omega + \langle \mathcal{T}_{\alpha,2} \mathbf{v}_{\alpha,2}, \mathbf{u}_{\partial,2} \rangle_{\partial\Omega}, & \text{for all } \mathbf{v}_{\alpha,2} \in H^{\mathcal{L}}(\Omega), \\ (\mathbf{v}_{\beta,2}, \mathcal{M}_\beta \partial_t \mathbf{e}_{\beta,2})_\Omega &= (\mathbf{v}_{\beta,2}, \mathcal{L} \mathbf{e}_{\alpha,2})_\Omega, & \text{for all } \mathbf{v}_{\beta,2} \in L^2(\Omega; \mathbb{B}), \\ \mathbf{y}_{\partial,2} &= \mathcal{T}_\alpha|_{\partial\Omega} \mathbf{e}_{\alpha,2}. \end{aligned} \quad (12)$$

Finite dimensional representation of the variables The two systems should not be discretized in the same manner, as different differential operators may arise in the weak formulations 11, 12. Consider a finite element Galerkin approximation of the test, trial and boundary input functions. For the two systems

$$\begin{aligned} \mathbf{v}_{\alpha,i} &\approx \sum_{k=1}^{n_{\alpha,i}} \chi_{\alpha,i}^k(\mathbf{x}) v_{\alpha,i}^k, & \mathbf{v}_{\beta,i} &\approx \sum_{k=1}^{n_{\beta,i}} \chi_{\beta,i}^k(\mathbf{x}) v_{\beta,i}^k, & \mathbf{u}_{\partial,i} &\approx \sum_{k=1}^{n_{\partial,i}} \chi_{\partial,i}^k(\mathbf{x}) u_{\partial,i}^k(t), \\ \mathbf{e}_{\alpha,i} &\approx \sum_{k=1}^{n_{\alpha,i}} \chi_{\alpha,i}^k(\mathbf{x}) e_{\alpha,i}^k(t), & \mathbf{e}_{\beta,i} &\approx \sum_{k=1}^{n_{\beta,i}} \chi_{\beta,i}^k(\mathbf{x}) e_{\beta,i}^k(t), & i &= \{1, 2\}. \end{aligned} \quad (13)$$

The finite element spaces associated to the state variables $\mathbf{e}_{\alpha,i}$, $\mathbf{e}_{\beta,i}$ are spanned by the basis functions

$$V_{\alpha,i} = \text{span}\{\chi_{\alpha,i}\}, \quad V_{\beta,i} = \text{span}\{\chi_{\beta,i}\}, \quad i = \{1, 2\}. \quad (14)$$

The guiding principle behind the choice of $V_{\alpha,i}$, $V_{\beta,i}$ is that of Hilbert complex.

Definition 2 (Hilbert Complex) A Hilbert complex is a sequence $\{H^k, \mathcal{L}^k\}_{k \in \mathbb{Z}}$ where:

- H^k are Hilbert spaces,
- $\mathcal{L}^k : H^k \rightarrow H^{k+1}$ are bounded linear operators,
- $\mathcal{L}^{k+1} \circ \mathcal{L}^k = 0$ for all $k \in \mathbb{Z}$.

Given an Hilbert complex it is possible to define the adjoint complex by using the definition of adjoint operator.

Example 2 (de-Rham Complex) One important example of an Hilbert complex that will be considered in Sec. 4 is the de-Rham complex

$$H^1(\Omega) \xrightarrow{\text{grad}} H^{\text{curl}}(\Omega) \xrightarrow{\text{curl}} H^{\text{div}}(\Omega) \xrightarrow{\text{div}} L^2(\Omega) \quad (15)$$

The adjoint complex reads

$$L^2(\Omega) \xleftarrow{\text{div}} \mathring{H}^{\text{div}}(\Omega) \xleftarrow{\text{curl}} \mathring{H}^{\text{curl}}(\Omega) \xleftarrow{\text{grad}} \mathring{H}^1(\Omega) \quad (16)$$

where the Hilbert spaces in the adjoint complex include homogeneous boundary conditions.

Finite element spaces $V_{\alpha,i}$, $V_{\beta,i}$ are chosen from a finite dimensional subcomplex.

Definition 3 (Hilbert Subcomplex) Given a Hilbert complex $\{H^k, \mathcal{L}^k\}_{k \in \mathbb{Z}}$, a subcomplex is a sequence of closed subspaces $\{V^k \subseteq H^k\}_{k \in \mathbb{Z}}$ such that:

- $\mathcal{L}^k(V^k) \subseteq V^{k+1}$ for all $k \in \mathbb{Z}$,
- V^k is a closed linear subspace of H^k ,
- The restriction of \mathcal{L}^k to V^k maps V^k to V^{k+1} .

In particular for systems (11), (12) the finite element spaces are selected in such a way that

$$\mathcal{L}^*(V_{\beta,1}) \subset V_{\alpha,1}, \quad \mathcal{L}(V_{\alpha,2}) \subset V_{\beta,2}. \quad (17)$$

The rationale behind the choice for the boundary spaces $V_{\partial,i} = \text{span}\{\chi_{\partial,i}\}$ will be clarified in Sec. (3).

Remark 2 (Equivalence with the second order formulation) Because of the inclusions (17), the mixed formulations coincides therefore with the second order formulation in time and space [17].

Algebraic realization for the case $\Gamma_1 = \partial\Omega$ In this case the formulation (11) includes only the input $\mathbf{u}_{\partial,1}$

$$\begin{aligned} \begin{bmatrix} \mathbf{M}_{\alpha,1} & 0 \\ 0 & \mathbf{M}_{\beta,1} \end{bmatrix} \frac{d}{dt} \begin{pmatrix} \mathbf{e}_{\alpha,1} \\ \mathbf{e}_{\beta,1} \end{pmatrix} &= \begin{bmatrix} 0 & -\mathbf{D}_{\mathcal{L}^*} \\ \mathbf{D}_{\mathcal{L}^*}^\top & 0 \end{bmatrix} \begin{pmatrix} \mathbf{e}_{\alpha,1} \\ \mathbf{e}_{\beta,1} \end{pmatrix} + \begin{bmatrix} 0 \\ \mathbf{B}_{\beta}^{\partial\Omega} \end{bmatrix} \mathbf{u}_{\partial,1}, \\ \mathbf{y}_{\partial,1} &= \begin{bmatrix} 0 & \mathbf{T}_{\beta}^{\partial\Omega} \end{bmatrix} \begin{pmatrix} \mathbf{e}_{\alpha,1} \\ \mathbf{e}_{\beta,1} \end{pmatrix}, \end{aligned} \quad (18)$$

where the matrices arising from the weak formulation are defined by

$$\begin{aligned} [\mathbf{M}_{\alpha,1}]_{ij} &= (\chi_{\alpha,1}^i, \mathcal{M}_{\alpha} \chi_{\alpha,1}^j)_{\Omega}, & [\mathbf{D}_{\mathcal{L}^*}]_{im} &= (\chi_{\alpha,1}^i, \mathcal{L}^* \chi_{\beta,1}^m)_{\Omega}, \\ [\mathbf{M}_{\beta,1}]_{mn} &= (\chi_{\beta,1}^m, \mathcal{M}_{\beta} \chi_{\beta,1}^n)_{\Omega}, & [\mathbf{B}_{\beta}^{\partial\Omega}]_{mk} &= \langle \mathcal{T}_{\beta} \chi_{\beta,1}^m, \chi_{\partial,1}^k \rangle_{\partial\Omega}. \end{aligned} \quad (19)$$

The trace matrix is a boolean matrix that localizes the degrees of freedom lying on the boundary

$$[\mathbf{T}_{\beta}^{\partial\Omega}]_{ki} = \begin{cases} 1, & \text{if } \mathcal{T}_{\beta} \chi_{\beta,1}^i \neq 0 \text{ on } \partial\Omega, \\ 0, & \text{otherwise.} \end{cases} \quad (20)$$

where $k = 1, \dots, \dim\{\mathcal{T}_{\beta} \chi_{\beta,1}^i \neq 0\}_1^{n_{\beta,1}}$ counts over the basis function lying on the boundary.

Algebraic realization for the case $\Gamma_2 = \partial\Omega$ In this case the formulation (12) includes the input $\mathbf{u}_{\partial,2}$ only, leading to the following system

$$\begin{aligned} \begin{bmatrix} \mathbf{M}_{\alpha,2} & 0 \\ 0 & \mathbf{M}_{\beta,2} \end{bmatrix} \frac{d}{dt} \begin{pmatrix} \mathbf{e}_{\alpha,2} \\ \mathbf{e}_{\beta,2} \end{pmatrix} &= \begin{bmatrix} 0 & -\mathbf{D}_{\mathcal{L}}^\top \\ \mathbf{D}_{\mathcal{L}} & 0 \end{bmatrix} \begin{pmatrix} \mathbf{e}_{\alpha,2} \\ \mathbf{e}_{\beta,2} \end{pmatrix} + \begin{bmatrix} \mathbf{B}_{\alpha}^{\partial\Omega} \\ 0 \end{bmatrix} \mathbf{u}_{\partial,2}, \\ \mathbf{y}_{\partial,2} &= \begin{bmatrix} 0 & \mathbf{T}_{\alpha}^{\partial\Omega} \end{bmatrix} \begin{pmatrix} \mathbf{e}_{\alpha,2} \\ \mathbf{e}_{\beta,2} \end{pmatrix} \end{aligned} \quad (21)$$

The matrices components are obtained as follows

$$\begin{aligned} [\mathbf{M}_{\alpha,2}]_{ij} &= (\chi_{\alpha,2}^i, \mathcal{M}_{\alpha} \chi_{\alpha,2}^j)_{\Omega}, & [\mathbf{D}_{\mathcal{L}}]_{mi} &= (\chi_{\beta,2}^m, \mathcal{L} \chi_{\alpha,2}^i)_{\Omega}, \\ [\mathbf{M}_{\beta,2}]_{mn} &= (\chi_{\beta,2}^m, \mathcal{M}_{\beta} \chi_{\beta,2}^n)_{\Omega}, & [\mathbf{B}_{\alpha}^{\partial\Omega}]_{ik} &= \langle \mathcal{T}_{\alpha} \chi_{\alpha,2}^i, \chi_{\beta,2}^k \rangle_{\partial\Omega}. \end{aligned} \quad (22)$$

For this system the trace matrix selects the degrees of freedom for the variable $\mathbf{e}_{\beta,2}$

$$[\mathbf{T}_{\alpha}^{\partial\Omega}]_{ki} = \begin{cases} 1, & \text{if } \mathcal{T}_{\alpha} \chi_{\alpha,2}^i \neq 0, \quad \text{on } \partial\Omega, \\ 0, & \text{otherwise.} \end{cases} \quad (23)$$

3 Domain Decomposition for mixed boundary conditions

The domain decomposition introduces an interface boundary Γ_{int} to split the domain $\Omega = \Omega_1 \cup \Omega_2$, where $\Omega_1 \cap \Omega_2 = \emptyset$ holds, such that the boundaries of the subdomains are given as $\partial\Omega_1 = \bar{\Gamma}_1 \cup \bar{\Gamma}_{\text{int}}$ and $\partial\Omega_2 = \bar{\Gamma}_2 \cup \bar{\Gamma}_{\text{int}}$ (cf. Fig 1). This interface boundary is chosen freely. The idea of the discretization is to use both formulations 11 and 12 concurrently to achieve natural boundary imposition for both boundary causalities. This means applying the formulations 11 to the Ω_1 subdomain and 12 to Ω_2 . To ensure proper coupling on the interface Γ_{int} consider the inputs and outputs from the port-Hamiltonian systems 31 and 32. The boundary inputs and outputs for Ω_1 include boundary condition for the problem and the input along the interconnection boundary

$$\begin{pmatrix} \mathbf{u}_{\partial,1} \\ \mathbf{u}_{\partial,1}^{\Gamma_{\text{int}}} \end{pmatrix} = \begin{bmatrix} \mathcal{T}_{\alpha}|_{\Gamma_1} & 0 \\ \mathcal{T}_{\alpha}|_{\Gamma_{\text{int}}} & 0 \end{bmatrix} \begin{pmatrix} \mathbf{e}_{\alpha} \\ \mathbf{e}_{\beta} \end{pmatrix}, \quad \begin{pmatrix} \mathbf{y}_{\partial,1} \\ \mathbf{y}_{\partial,1}^{\Gamma_{\text{int}}} \end{pmatrix} = \begin{bmatrix} 0 & \mathcal{T}_{\beta}|_{\Gamma_1} \\ 0 & \mathcal{T}_{\beta}|_{\Gamma_{\text{int}}} \end{bmatrix} \begin{pmatrix} \mathbf{e}_{\alpha} \\ \mathbf{e}_{\beta} \end{pmatrix}. \quad (24)$$

For the Ω_2 domain one input will be the actual boundary condition and a second input represent the exchange of information along the interface

$$\begin{pmatrix} \mathbf{u}_{\partial,2} \\ \mathbf{u}_{\partial,2}^{\Gamma_{\text{int}}} \end{pmatrix} = \begin{bmatrix} 0 & \mathcal{T}_{\beta}|_{\Gamma_2} \\ 0 & \mathcal{T}_{\beta}|_{\Gamma_{\text{int}}} \end{bmatrix} \begin{pmatrix} \mathbf{e}_{\alpha} \\ \mathbf{e}_{\beta} \end{pmatrix}, \quad \begin{pmatrix} \mathbf{y}_{\partial,2} \\ \mathbf{y}_{\partial,2}^{\Gamma_{\text{int}}} \end{pmatrix} = \begin{bmatrix} \mathcal{T}_{\alpha}|_{\Gamma_2} & 0 \\ \mathcal{T}_{\alpha}|_{\Gamma_{\text{int}}} & 0 \end{bmatrix} \begin{pmatrix} \mathbf{e}_{\alpha} \\ \mathbf{e}_{\beta} \end{pmatrix}. \quad (25)$$

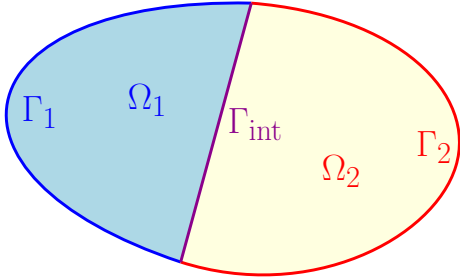


Figure 1: Splitting of the domain.

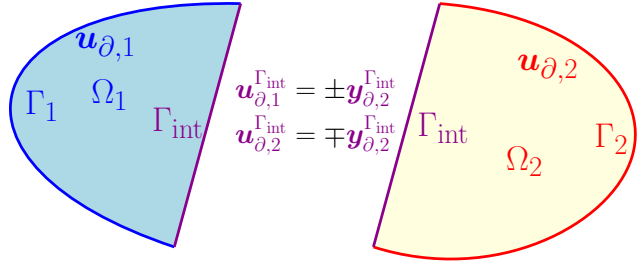


Figure 2: Interconnection at the interface Γ_{12} .

The coupling of the two domain takes place on Γ_{int} because the inputs and outputs are related by

$$\begin{aligned} \mathbf{u}_{\partial,1}^{\Gamma_{\text{int}}} &= \pm \mathbf{y}_{\partial,2}^{\Gamma_{\text{int}}}, \\ \mathbf{u}_{\partial,2}^{\Gamma_{\text{int}}} &= \mp \mathbf{y}_{\partial,1}^{\Gamma_{\text{int}}}, \end{aligned} \quad (26)$$

as shown in Figure 2. The \pm and \mp are used due to opposite outward unit normals depending on the domain. The correct boundary causality is achieved by integrating the \mathcal{L} term by parts on Ω_1 , based on the weak form 11, and the \mathcal{L}^* on the Ω_2 subdomain, based on the weak form 12. Consider the additivity of integral operator, the boundary term $\langle \mathcal{T}_{\partial,\beta} \mathbf{v}_{\beta}, \mathbf{u}_{\partial} \rangle_{\partial\Omega}$ from the Ω_1 domain becomes

$$\langle \mathcal{T}_{\beta} \mathbf{v}_{\beta}, \mathcal{T}_{\alpha} \mathbf{e}_{\alpha} \rangle_{\partial\Omega_1} = \langle \mathcal{T}_{\beta} \mathbf{v}_{\beta}, \mathbf{u}_{\partial,1} \rangle_{\Gamma_1} + \langle \mathcal{T}_{\beta} \mathbf{v}_{\beta}, \mathbf{u}_{\partial,1}^{\Gamma_{\text{int}}} \rangle_{\Gamma_{\text{int}}}, \quad (27)$$

while for the Ω_2 subdomain

$$\langle \mathcal{T}_\alpha \mathbf{v}_\alpha, \mathcal{T}_\beta \mathbf{e}_\beta \rangle_{\partial\Omega_2} = \langle \mathcal{T}_\alpha \mathbf{v}_\alpha, \mathbf{u}_{\partial,2} \rangle_{\Gamma_2} + \langle \mathcal{T}_\alpha \mathbf{v}_\alpha, \mathbf{u}_{\partial,2}^{\Gamma_{\text{int}}} \rangle_{\Gamma_{\text{int}}}. \quad (28)$$

The weak formulation for Ω_1 is to find $\mathbf{e}_\alpha \in L^2(\Omega_1; \mathbb{A})$, $\mathbf{e}_\beta \in H^{\mathcal{L}^*}(\Omega_1)$ such that $\forall \mathbf{v}_\alpha \in L^2(\Omega_2; \mathbb{A})$ and $\forall \mathbf{v}_\beta \in H^{\mathcal{L}^*}(\Omega_1)$ it holds

$$\begin{aligned} (\mathbf{v}_\alpha, \mathcal{M}_\alpha \partial_t \mathbf{e}_\alpha)_{\Omega_1} &= -(\mathbf{v}_\alpha, \mathcal{L}^* \mathbf{e}_\beta)_{\Omega_1}, \\ (\mathbf{v}_\alpha, \mathcal{M}_\beta \partial_t \mathbf{e}_\beta)_{\Omega_1} &= (\mathcal{L}^* \mathbf{v}_\beta, \mathbf{e}_\alpha)_{\Omega_1} + \langle \mathcal{T}_\beta \mathbf{v}_\beta, \mathbf{u}_{\partial,1} \rangle_{\Gamma_1} + \langle \mathcal{T}_\beta \mathbf{v}_\beta, \mathbf{u}_{\partial,1}^{\Gamma_{\text{int}}} \rangle_{\Gamma_{\text{int}}}, \end{aligned} \quad (29)$$

where the boundary control and trace matrices are now restricted on the subpartitions of the boundary Γ_{int} . For the Ω_2 subdomain with 28 find $\mathbf{e}_\alpha \in H^{\mathcal{L}}(\Omega_2)$, $\mathbf{e}_\beta \in L^2(\Omega_2; \mathbb{B})$ that satisfy $\forall \mathbf{v}_\alpha \in H^{\mathcal{L}}(\Omega_2)$ and $\forall \mathbf{v}_\beta \in L^2(\Omega_2; \mathbb{B})$

$$\begin{aligned} (\mathbf{v}_\alpha, \mathcal{M}_\alpha \partial_t \mathbf{e}_\alpha)_{\Omega_2} &= -(\mathcal{L} \mathbf{v}_\alpha, \mathbf{e}_\beta)_{\Omega_2} + \langle \mathcal{T}_\alpha \mathbf{v}_\alpha, \mathbf{u}_{\partial,2} \rangle_{\Gamma_2} + \langle \mathcal{T}_\alpha \mathbf{v}_\alpha, \mathbf{u}_{\partial,2}^{\Gamma_{\text{int}}} \rangle_{\Gamma_{\text{int}}}, \\ (\mathbf{v}_\beta, \mathcal{M}_\beta \partial_t \mathbf{e}_\beta)_{\Omega_2} &= (\mathbf{v}_\beta, \mathcal{L} \mathbf{e}_\alpha)_{\Omega_2} \end{aligned} \quad (30)$$

The weak formulation can be discretized using the basis functions as in 13 where e.g. $\mathbf{e}_{\alpha,1}$ denotes \mathbf{e}_α on Ω_1 , to include the decomposed domain and interface. Using the basis functions, the formulations for each subdomain can be written into a finite dimensional form. For Ω_1 this becomes

$$\begin{aligned} \begin{bmatrix} \mathbf{M}_{\alpha,1} & 0 \\ 0 & \mathbf{M}_{\beta,1} \end{bmatrix} \frac{d}{dt} \begin{pmatrix} \mathbf{e}_{\alpha,1} \\ \mathbf{e}_{\beta,1} \end{pmatrix} &= \begin{bmatrix} 0 & -\mathbf{D}_{\mathcal{L}^*} \\ \mathbf{D}_{\mathcal{L}^*}^\top & 0 \end{bmatrix} \begin{pmatrix} \mathbf{e}_{\alpha,1} \\ \mathbf{e}_{\beta,1} \end{pmatrix} + \begin{bmatrix} 0 & 0 \\ \mathbf{B}_\beta^{\Gamma_1} & \mathbf{B}_\beta^{\Gamma_{\text{int}}} \end{bmatrix} \begin{pmatrix} \mathbf{u}_{\partial,1} \\ \mathbf{u}_{\partial,1}^{\Gamma_{\text{int}}} \end{pmatrix}, \\ \begin{pmatrix} \mathbf{y}_{\partial,1} \\ \mathbf{y}_{\partial,1}^{\Gamma_{\text{int}}} \end{pmatrix} &= \begin{bmatrix} 0 & \mathbf{T}_\beta^{\Gamma_1} \\ 0 & \mathbf{T}_\beta^{\Gamma_{\text{int}}} \end{bmatrix} \begin{pmatrix} \mathbf{e}_{\alpha,1} \\ \mathbf{e}_{\beta,1} \end{pmatrix}. \end{aligned} \quad (31)$$

where the output variables are computed strongly considering discrete trace operators. In an analogous manner for Ω_2 it is obtained

$$\begin{aligned} \begin{bmatrix} \mathbf{M}_{\alpha,2} & 0 \\ 0 & \mathbf{M}_{\beta,2} \end{bmatrix} \frac{d}{dt} \begin{pmatrix} \mathbf{e}_{\alpha,2} \\ \mathbf{e}_{\beta,2} \end{pmatrix} &= \begin{bmatrix} 0 & -\mathbf{D}_{\mathcal{L}}^\top \\ \mathbf{D}_{\mathcal{L}} & 0 \end{bmatrix} \begin{pmatrix} \mathbf{e}_{\alpha,2} \\ \mathbf{e}_{\beta,2} \end{pmatrix} + \begin{bmatrix} \mathbf{B}_\alpha^{\Gamma_2} & \mathbf{B}_\alpha^{\Gamma_{\text{int}}} \\ 0 & 0 \end{bmatrix} \begin{pmatrix} \mathbf{u}_{\partial,2} \\ \mathbf{u}_{\partial,2}^{\Gamma_{\text{int}}} \end{pmatrix}, \\ \begin{pmatrix} \mathbf{y}_{\partial,2} \\ \mathbf{y}_{\partial,2}^{\Gamma_{\text{int}}} \end{pmatrix} &= \begin{bmatrix} \mathbf{T}_\alpha^{\Gamma_2} & 0 \\ \mathbf{T}_\alpha^{\Gamma_{\text{int}}} & 0 \end{bmatrix} \begin{pmatrix} \mathbf{e}_{\alpha,2} \\ \mathbf{e}_{\beta,2} \end{pmatrix}. \end{aligned} \quad (32)$$

Choice of the boundary functions The boundary shape functions are not chosen in a independent way with respect to the state variables. Given Eqs. (24), (25) and (26), it is natural to choose the basis functions for the inputs as being the basis function of the associated co-energy variable on the boundary subpartitions. Following the methodology detailed in [18], the basis functions for the inputs of the primal system are taken to be the trace of the associated variable in the dual system and viceversa

$$\begin{aligned} \text{span}\{\chi_{\partial,1}\}|_{\partial\Omega_1} &= \text{span}\{\mathcal{T}_\alpha|_{\partial\Omega_1} \chi_{\alpha,2}\}, \\ \text{span}\{\chi_{\partial,2}\}|_{\partial\Omega_2} &= \text{span}\{\mathcal{T}_\beta|_{\partial\Omega_2} \chi_{\beta,1}\}. \end{aligned} \quad (33)$$

This choice will couple the two systems and is important for the domain decomposition strategy. The relations in Eq. (33) provide the interconnection of the two system on Γ_{int}

$$\begin{aligned} \mathbf{u}_{\partial,1}^{\Gamma_{\text{int}}} &= \pm \mathbf{y}_{\partial,2}^{\Gamma_{\text{int}}} = \pm \mathbf{T}_\alpha^{\Gamma_{\text{int}}} \mathbf{e}_{\alpha,2}, \\ \mathbf{u}_{\partial,2}^{\Gamma_{\text{int}}} &= \mp \mathbf{y}_{\partial,1}^{\Gamma_{\text{int}}} = \pm \mathbf{T}_\beta^{\Gamma_{\text{int}}} \mathbf{e}_{\beta,1}. \end{aligned} \quad (34)$$

These equations represents a feedback interconnection (cf. Fig. 3) which in port-Hamiltonian systems jargon is also called a gyrator interconnection. Relations (33) are also responsible for a factorization of the \mathbf{B} matrices

$$\mathbf{B}_\alpha^{\Gamma_{\text{int}}} = (\mathbf{T}_\alpha^{\Gamma_{\text{int}}})^\top \mathbf{\Psi}^{\Gamma_{\text{int}}}, \quad \mathbf{B}_\beta^{\Gamma_{\text{int}}} = (\mathbf{T}_\beta^{\Gamma_{\text{int}}})^\top (\mathbf{\Psi}^{\Gamma_{\text{int}}})^\top, \quad (35)$$

where $[\mathbf{\Psi}^{\Gamma_{\text{int}}}]_{lk} = \langle \chi_{\partial,1}^l, \chi_{\partial,2}^k \rangle_{\Gamma_{\text{int}}}$.

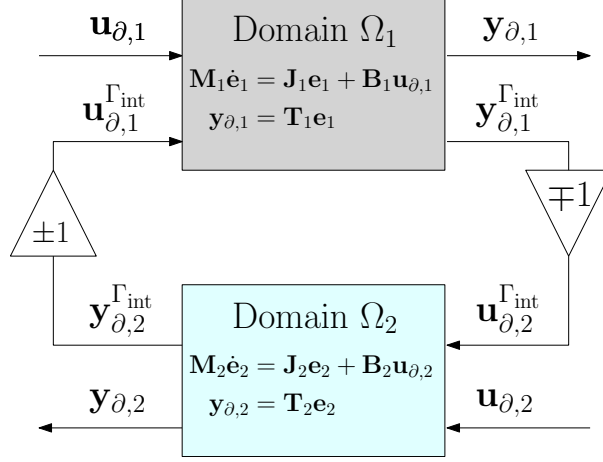


Figure 3: Feedback interconnection of the two systems arising from the domain decomposition.

The systems found for Ω_1 and Ω_2 can be combined into a monolithic interconnected system for the entire domain Ω . The pH-system for the full domain is provided as

$$\text{Diag} \begin{bmatrix} \mathbf{M}_{\alpha,1} \\ \mathbf{M}_{\beta,1} \\ \mathbf{M}_{\alpha,2} \\ \mathbf{M}_{\beta,2} \end{bmatrix} \frac{d}{dt} \begin{pmatrix} \mathbf{e}_{\alpha,1} \\ \mathbf{e}_{\beta,1} \\ \mathbf{e}_{\alpha,2} \\ \mathbf{e}_{\beta,2} \end{pmatrix} = \begin{bmatrix} 0 & -\mathbf{D}_{\mathcal{L}^*} & 0 & 0 \\ \mathbf{D}_{\mathcal{L}^*}^\top & 0 & \pm \mathbf{L}^{\Gamma_{int}} & 0 \\ 0 & \mp (\mathbf{L}^{\Gamma_{int}})^\top & 0 & -\mathbf{D}_{\mathcal{L}}^\top \\ 0 & 0 & \mathbf{D}_{\mathcal{L}} & 0 \end{bmatrix} \begin{pmatrix} \mathbf{e}_{\alpha,1} \\ \mathbf{e}_{\beta,1} \\ \mathbf{e}_{\alpha,2} \\ \mathbf{e}_{\beta,2} \end{pmatrix} + \begin{bmatrix} 0 & 0 \\ \mathbf{B}_{\beta}^{\Gamma_1} & 0 \\ 0 & \mathbf{B}_{\alpha}^{\Gamma_2} \\ 0 & 0 \end{bmatrix} \begin{pmatrix} \mathbf{u}_{\partial,1} \\ \mathbf{u}_{\partial,2} \end{pmatrix},$$

$$\begin{pmatrix} \mathbf{y}_{\partial,1} \\ \mathbf{y}_{\partial,2} \end{pmatrix} = \begin{bmatrix} 0 & \mathbf{T}_{\beta}^{\Gamma_1} & 0 & 0 \\ 0 & 0 & \mathbf{T}_{\alpha}^{\Gamma_2} & 0 \end{bmatrix} \begin{pmatrix} \mathbf{e}_{\alpha,1} \\ \mathbf{e}_{\beta,1} \\ \mathbf{e}_{\alpha,2} \\ \mathbf{e}_{\beta,2} \end{pmatrix}. \tag{36}$$

where $\mathbf{L}^{\Gamma_{int}} = (\Psi^{\Gamma_{int}} \mathbf{T}_{\beta}^{\Gamma_{int}})^\top \mathbf{T}_{\alpha}^{\Gamma_{int}}$. The structure of the system is again Hamiltonian and can be written compactly as

$$\begin{aligned} \mathbf{M} \dot{\mathbf{e}} &= \mathbf{J} \mathbf{e} + \mathbf{B} \mathbf{u}, \\ \mathbf{y} &= \mathbf{T} \mathbf{e}. \end{aligned} \tag{37}$$

where $\mathbf{J} = -\mathbf{J}^\top$ is skew-symmetric.

Time integration with a staggered implicit midpoint scheme The system of equations in 36 can be solved in monolithically, in a partitioned way or using a combined strategy. In this work the latter approach is adopted. An implicit integrator is used for each subdomain and the two systems are coupled using a partitioned strategy to reduce the overall computational cost. The scheme used is such to preserve the overall symplectic Hamiltonian structure [23]. For each subdomain Ω_1 , Ω_2 an implicit-midpoint scheme is chosen and the coupling between the two is performed by means of a Störmer Verlet scheme (or also known as leapfrog method in the PDE community). To illustrate the time integration algorithm, consider the two system to be solved

$$\begin{aligned} \mathbf{M}_1 \dot{\mathbf{e}}_1 &= \mathbf{J}_1 \mathbf{e}_1 + \mathbf{G} \mathbf{e}_2 + \mathbf{B}_1 \mathbf{u}_1, & \text{Domain } \Omega_1, \\ \mathbf{M}_2 \dot{\mathbf{e}}_2 &= \mathbf{J}_2 \mathbf{e}_2 - \mathbf{G}^\top \mathbf{e}_1 + \mathbf{B}_2 \mathbf{u}_2, & \text{Domain } \Omega_2. \end{aligned}$$

For domain Ω_1 variables are sampled at integers time instants, where for Ω_2 they are sampled at half integers instants

$$\dot{\mathbf{e}}_1 \approx \frac{\mathbf{e}_1^{n+1} - \mathbf{e}_1^n}{\Delta t}, \quad \dot{\mathbf{e}}_2 \approx \frac{\mathbf{e}_2^{n+\frac{1}{2}} - \mathbf{e}_2^{n-\frac{1}{2}}}{\Delta t} \tag{38}$$

Each system is solved using an implicit midpoint method, where the right-hand side is evaluated at the midpoint of the time interval Δt (for linear system this integrator corresponds

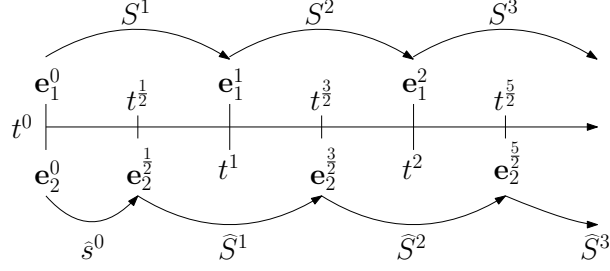


Figure 4: Illustration of time integration system and staggering between the two subdomains Ω_1 and Ω_2 .

to the Crank-Nicholson scheme). Since the two system are staggered, the coupling becomes explicit

$$\begin{aligned} \mathbf{M}_1 \left(\frac{\mathbf{e}_1^{n+1} - \mathbf{e}_1^n}{\Delta t} \right) &= \mathbf{J}_1 \left(\frac{\mathbf{e}_1^n + \mathbf{e}_1^{n+1}}{2} \right) + \mathbf{L}\mathbf{e}_2^{n+\frac{1}{2}} + \mathbf{B}_1\mathbf{u}_1^{n+\frac{1}{2}}, \\ \mathbf{M}_2 \left(\frac{\mathbf{e}_2^{n+\frac{1}{2}} - \mathbf{e}_2^{n-\frac{1}{2}}}{\Delta t} \right) &= \mathbf{J}_2 \left(\frac{\mathbf{e}_2^{n+\frac{1}{2}} + \mathbf{e}_2^{n-\frac{1}{2}}}{2} \right) - \mathbf{L}^\top \mathbf{e}_1^n + \mathbf{B}_2\mathbf{u}_2^n. \end{aligned}$$

The next value for the state can be obtained as follows

$$\begin{cases} \text{Step } S^n & \left(\mathbf{M}_1 - \frac{\Delta t}{2} \mathbf{J}_1 \right) \mathbf{e}_1^{n+1} = \left(\mathbf{M}_1 + \frac{\Delta t}{2} \mathbf{J}_1 \right) \mathbf{e}_1^n + \Delta t (\mathbf{L}\mathbf{e}_2^{n+\frac{1}{2}} + \mathbf{B}_1\mathbf{u}_1^{n+\frac{1}{2}}), \\ \text{Step } \widehat{S}^n & \left(\mathbf{M}_2 - \frac{\Delta t}{2} \mathbf{J}_2 \right) \mathbf{e}_2^{n+\frac{1}{2}} = \left(\mathbf{M}_2 + \frac{\Delta t}{2} \mathbf{J}_2 \right) \mathbf{e}_2^{n-\frac{1}{2}} + \Delta t (-\mathbf{L}^\top \mathbf{e}_1^n + \mathbf{B}_2\mathbf{u}_2^n), \end{cases} \quad (39)$$

In order to start the iteration value $\mathbf{e}_2^{\frac{1}{2}}$ needs to be computed. An explicit Euler method is used to compute this value

$$\text{Step } \widehat{S}^0 \quad \mathbf{M}_2 \mathbf{e}_2^{\frac{1}{2}} = (\mathbf{M}_2 + \Delta t \mathbf{J}_2) \mathbf{e}_2^0 + \Delta t (-\mathbf{L}^\top \mathbf{e}_1^0 + \mathbf{B}_2 \mathbf{u}_2^0).$$

The numerical scheme is illustrated in Fig 4.

4 Numerical examples

In this section we apply the domain decomposition strategy to three different examples:

- the one dimensional Euler-Bernoulli beam model;
- the two dimensional wave equation;
- the three dimensional Maxwell equations.

The decomposition of the mesh has been implemented using GMSH [24]. All the investigations will be performed employing the finite element library FIREDRAKE [25]. The staggered implicit midpoint integration as described in Section 2 has been used for the temporal part of the problem with a time step of $\Delta t = 0.001$ for all simulations.

4.1 Euler-Bernoulli beam in 1D

In this example a one dimensional beam with length L under a Neumann boundary condition at $x = 0$ (a force and torque are imposed at this point) and a Dirichlet boundary condition at $x = L$ (the velocity and rotation are imposed at this point), is decomposed into two subdomains Ω_2 and Ω_1 using an interface vertex Γ_{int} located at $x_{\text{int}} = L/2$, cf. Figure 5 for a visual representation. The displacements of the Euler-Bernoulli beam are described by a second order time derivative and a fourth order spatial derivative as

$$\rho A \partial_{tt} w + EI \partial_{xxxx} w = 0, \quad (40)$$

where w is the displacement. The Euler-Bernoulli equation 40 can be expressed in terms of the energy variable with

$$e_\alpha = \partial_t w, \quad e_\beta = EI \partial_{xx} w. \quad (41)$$

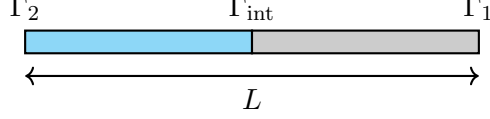


Figure 5: The decomposed Euler-Bernoulli beam with mixed boundary conditions.

The energy variables are related to the co-energy variables by System 5. For the Euler-Bernoulli beam, considering the energy variables from 41, the system becomes

$$\begin{bmatrix} \rho A & 0 \\ 0 & (EI)^{-1} \end{bmatrix} \begin{pmatrix} \partial_t e_\alpha \\ \partial_t e_\beta \end{pmatrix} = \begin{bmatrix} 0 & -\partial_{xx} \\ \partial_{xx} & 0 \end{bmatrix} \begin{pmatrix} e_\alpha \\ e_\beta \end{pmatrix}, \quad (42)$$

where the linear differential operator \mathcal{L} is now ∂_{xx} , and so is its formal adjoint \mathcal{L}^* as ∂_{xx} is self-adjoint. Now there are indeed two possibilities for applying integration by parts, namely 11 and 12, leading to the weak formulations detailed in Eqs. 29 and 30. For the subdomain with the Dirichlet boundary condition Ω_1 , the weak formulation is as follows. Find $e_\alpha \in H^2(\Omega_1)$, $e_\beta \in L^2(\Omega_1)$ such that $\forall v_\alpha \in H^2(\Omega_1)$ and $\forall v_\beta \in L^2(\Omega_1)$

$$\begin{aligned} (v_\alpha, \rho A \partial_t e_\alpha)_{\Omega_1} &= -(v_\alpha, \partial_{xx} e_\beta)_{\Omega_1}, \\ (v_\alpha, (EI)^{-1} \partial_t e_\beta)_{\Omega_1} &= (\partial_{xx} v_\beta, e_\alpha)_{\Omega_1} + \langle \mathcal{T}_\beta v_\beta, u_{\partial,1} \rangle_{\Gamma_1} + \langle \mathcal{T}_\beta v_\beta, u_{\partial,1}^{\Gamma_{\text{int}}} \rangle_{\Gamma_{\text{int}}}, \end{aligned} \quad (43)$$

where the trace operator $\mathcal{T}_\beta : H^2([a, b]) \rightarrow \mathbb{R}^4$ is given by

$$\mathcal{T}_\beta f = \begin{pmatrix} -\partial_x f(b) & \partial_x f(a) & f(b) & -f(a) \end{pmatrix}^\top.$$

For the other subdomain Ω_2 , the weak formulation is: find $e_\alpha \in L^2(\Omega_2)$, $e_\beta \in H^2(\Omega_2)$ such that $\forall v_\alpha \in L^2(\Omega_2)$ and $\forall v_\beta \in H^2(\Omega_2)$ it holds

$$\begin{aligned} (v_\alpha, \rho A \partial_t e_\alpha)_{\Omega_2} &= -(\partial_{xx} v_\alpha, e_\beta)_{\Omega_2} + \langle \mathcal{T}_\alpha v_\alpha, u_{\partial,2} \rangle_{\Gamma_2} + \langle \mathcal{T}_\alpha v_\alpha, u_{\partial,2}^{\Gamma_{\text{int}}} \rangle_{\Gamma_{\text{int}}}, \\ (v_\beta, (EI)^{-1} \partial_t e_\beta)_{\Omega_2} &= (v_\beta, \partial_{xx} e_\alpha)_{\Omega_2}, \end{aligned} \quad (44)$$

where the trace operator $\mathcal{T}_\alpha : H^2([a, b]) \rightarrow \mathbb{R}^4$ is given by

$$\mathcal{T}_\alpha f = \begin{pmatrix} f(b) & -f(a) & -\partial_x f(b) & \partial_x f(a) \end{pmatrix}^\top.$$

The port-Hamiltonian systems with its outputs are taken from 31 and 32 for the subdomains Ω_1 and Ω_2 respectively, as

$$\begin{aligned} \begin{bmatrix} \mathbf{M}_{\alpha,1} & 0 \\ 0 & \mathbf{M}_{\beta,1} \end{bmatrix} \frac{d}{dt} \begin{pmatrix} \mathbf{e}_{\alpha,1} \\ \mathbf{e}_{\beta,1} \end{pmatrix} &= \begin{bmatrix} 0 & -\mathbf{D}_{\partial_{xx}} \\ \mathbf{D}_{\partial_{xx}}^\top & 0 \end{bmatrix} \begin{pmatrix} \mathbf{e}_{\alpha,1} \\ \mathbf{e}_{\beta,1} \end{pmatrix} + \begin{bmatrix} 0 & 0 \\ \mathbf{B}_\beta^{\Gamma_1} & \mathbf{B}_\beta^{\Gamma_{\text{int}}} \end{bmatrix} \begin{pmatrix} \mathbf{u}_{\partial,1} \\ \mathbf{u}_{\partial,1}^{\text{int}} \end{pmatrix}, \\ \begin{pmatrix} \mathbf{y}_{\partial,1} \\ \mathbf{y}_{\partial,1}^{\text{int}} \end{pmatrix} &= \begin{bmatrix} 0 & \mathbf{T}_\beta^{\Gamma_1} \\ 0 & \mathbf{T}_\beta^{\Gamma_{\text{int}}} \end{bmatrix} \begin{pmatrix} \mathbf{e}_{\alpha,1} \\ \mathbf{e}_{\beta,1} \end{pmatrix}, \end{aligned} \quad (45)$$

for the Ω_1 domain. For the Ω_2 subdomain the pH-system is given as

$$\begin{aligned} \begin{bmatrix} \mathbf{M}_{\alpha,2} & 0 \\ 0 & \mathbf{M}_{\beta,2} \end{bmatrix} \frac{d}{dt} \begin{pmatrix} \mathbf{e}_{\alpha,2} \\ \mathbf{e}_{\beta,2} \end{pmatrix} &= \begin{bmatrix} 0 & \mathbf{D}_{\partial_{xx}}^\top \\ -\mathbf{D}_{\partial_{xx}} & 0 \end{bmatrix} \begin{pmatrix} \mathbf{e}_{\alpha,2} \\ \mathbf{e}_{\beta,2} \end{pmatrix} + \begin{bmatrix} \mathbf{B}_\alpha^{\Gamma_2} & \mathbf{B}_\alpha^{\Gamma_{\text{int}}} \\ 0 & 0 \end{bmatrix} \begin{pmatrix} \mathbf{u}_{\partial,2} \\ \mathbf{u}_{\partial,2}^{\text{int}} \end{pmatrix}, \\ \begin{pmatrix} \mathbf{y}_{\partial,2} \\ \mathbf{y}_{\partial,2}^{\text{int}} \end{pmatrix} &= \begin{bmatrix} \mathbf{T}_\alpha^{\Gamma_2} & 0 \\ \mathbf{T}_\alpha^{\Gamma_{\text{int}}} & 0 \end{bmatrix} \begin{pmatrix} \mathbf{e}_{\alpha,2} \\ \mathbf{e}_{\beta,2} \end{pmatrix}. \end{aligned} \quad (46)$$

Case study The proposed discretization is applied to a beam of length with boundary conditions given by

$$\begin{aligned} \text{Neumann condition,} \quad e_\beta|_{x=0} &= EI \partial_{xx} w_{\text{ex}}(0, t), & \partial_x e_\beta|_{x=0} &= EI \partial_{xxx} w_{\text{ex}}(0, t), \\ \text{Dirichlet condition,} \quad e_\alpha|_{x=L} &= \partial_t w_{\text{ex}}(L, t) & \partial_x e_\alpha|_{x=L} &= \partial_t \partial_x w_{\text{ex}}(L, t), \end{aligned} \quad (47)$$

where w_{ex} is the exact solution to the Euler-Bernoulli beam problem is provided by [26, Chapter 12] as

$$w_{\text{ex}}(x, t) = \frac{1}{2} [\cosh(\sqrt{\omega}x) + \cos(\sqrt{\omega}x)] \sin(\omega t). \quad (48)$$

Finite element bases Similar to the decomposition of the domain, the one dimensional mesh (an interval) is constructed as a union of the subdomain meshes as $\mathcal{I}_h = \mathcal{I}_h^{\Omega_1} \cup \mathcal{I}_h^{\Omega_2}$, where the superscripts denote the subdomains. The finite element family used to solve the Euler-Bernoulli beam are the Discontinuous Galerkin elements of order 1 (DG₁) to discretize the L^2 space, and the Hermite (Her) elements to discretize the H^2 space, though the mixed finite element spaces are different on each subdomain. This choice is justified by the Bernstein–Gelfand–Gelfand sequences [27]. The idea of this construction is to consider multiple copies of the de-Rham complex and connect them via algebraic operators. The Euler-Bernoulli beam example constitutes the simplest example of this construction with the following diagram

$$\begin{array}{ccc} H^2 & \xrightarrow{\partial_x} & H^1 \\ & \nearrow I & \\ H^1 & \xrightarrow{\partial_x} & L^2 \end{array}$$

where H^i is Sobolev spaces of functions with square integrable i -th derivative and I is the identity (which is bijective). The following complex and the considered finite element subcomplex is given by

$$\begin{array}{ccc} H^2 & \xrightarrow{\partial_{xx}^2} & L^2 \\ \downarrow \Pi & & \downarrow \Pi \\ \text{Her} & \xrightarrow{\partial_{xx}^2} & \text{DG}_1 \end{array}$$

Other construction based on splines are possible. Therefore, for the $\mathcal{I}_h^{\Omega_1}$ domain the finite dimensional spaces are

$$\begin{aligned} V_{\alpha,1} &= \{u_h \in L^2(\Omega_1) \mid \forall E \in \mathcal{I}_h^{\Omega_1}, u_h|_E \in \text{DG}_1\}, \\ V_{\beta,1} &= \{u_h \in H^2(\Omega_1) \mid \forall E \in \mathcal{I}_h^{\Omega_1}, u_h|_E \in \text{Her}\}. \end{aligned}$$

For the $\mathcal{I}_h^{\Omega_2}$ domain the finite dimensional spaces are

$$\begin{aligned} V_{\alpha,2} &= \{u_h \in H^2(\Omega_2) \mid \forall E \in \mathcal{I}_h^{\Omega_2}, u_h|_E \in \text{Her}\}, \\ V_{\beta,2} &= \{u_h \in L^2(\Omega_2) \mid \forall E \in \mathcal{I}_h^{\Omega_2}, u_h|_E \in \text{DG}_1\}. \end{aligned}$$

Results The results are shown for a beam with properties $EI = 1$, $\rho A = 1$, $L = 1$ and frequency given by $\omega = 4$. The domain is discretized using three elements for both $\mathcal{I}_h^{\Omega_1}$ and $\mathcal{I}_h^{\Omega_2}$ for a total of $n_{el} = 6$ elements for \mathcal{I}_h . The vertical velocity and vertical displacement at $x = 0$ of the beam have been plotted in Figure 6. The numerical solution is seen to match perfectly with the exact solutions for both the velocity and the displacement. The numerical solution for the entire beam's position over time is provided in Figure 7, together with the exact solution at $x = 0$ and $x = L$. On the first half of the beam, i.e. $x < 0.5L$, there seem to be more elements present. This is due to the plotting the multiple degrees of freedom present in the Hermite elements, i.e. the Hermite elements use a polynomial degree of 3, while the DG elements has a degree of 1.

4.2 The Wave Equation in 2D

In this section we study the method for the two dimensional wave equation on a unit square domain

$$\partial_{tt}\phi - \text{div grad } \phi = 0, \quad \Omega = [0, 1]^2, \quad (49)$$

split into subdomains Ω_1 and Ω_2 with a Dirichlet boundary condition on Γ_1 and a Neumann boundary condition on Γ_2 . The discretization of the wave equation starts again by expressing via the variables

$$\alpha = \partial_t \phi, \quad \beta = \text{grad } \phi. \quad (50)$$

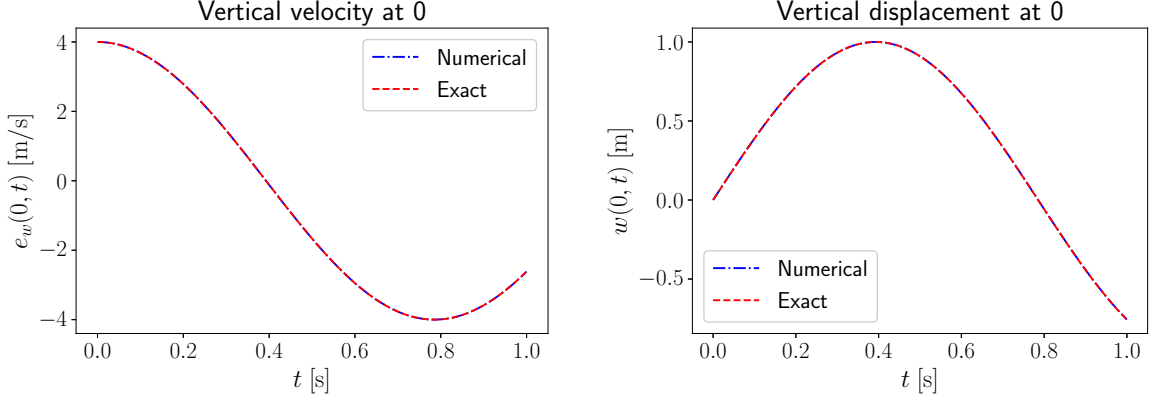


Figure 6: Analytical and numerical solutions for the Euler-Bernoulli beam.

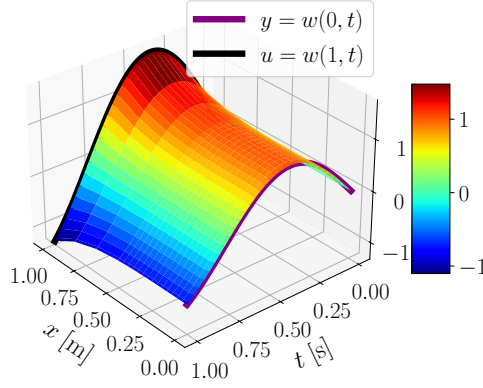


Figure 7: Displacements along the beam over time.

The system equivalent to 5 is then written as

$$\begin{pmatrix} \partial_t \boldsymbol{\alpha} \\ \partial_t \boldsymbol{\beta} \end{pmatrix} = \begin{bmatrix} 0 & \text{div} \\ \text{grad} & 0 \end{bmatrix} \begin{pmatrix} \mathbf{e}_\alpha \\ \mathbf{e}_\beta \end{pmatrix}, \quad (51)$$

so the differential operator for the wave equations is $\mathcal{L} = \text{grad}$ and its formal adjoint is now $\mathcal{L}^* = -\text{div}$. The discretization is obtained by multiplying by the test functions and applying integration by parts as in 11 or 12. The resulting weak formulation for Ω_1 is to find $\mathbf{e}_\alpha \in L^2(\Omega_1)$ and $\mathbf{e}_\beta \in H^{\text{div}}(\Omega_1)$ such that $\forall v_\alpha \in L^2(\Omega_1)$ and $\forall \mathbf{v}_\beta \in H^{\text{div}}(\Omega_1)$ it holds

$$\begin{aligned} (v_\alpha, \partial_t e_\alpha)_{\Omega_1} &= -(v_\alpha, \text{div } \mathbf{e}_\beta)_{\Omega_1}, \\ (\mathbf{v}_\beta, \partial_t \mathbf{e}_\beta)_{\Omega_1} &= (\text{div } \mathbf{v}_\beta, \mathbf{e}_\alpha)_{\Omega_1} + \langle \mathcal{T}_\beta \mathbf{v}_\beta, u_{\partial,1} \rangle_{\Gamma_1} + \langle \mathcal{T}_\beta \mathbf{v}_\beta, u_{\partial,1}^{\Gamma_{\text{int}}} \rangle_{\Gamma_{\text{int}}}, \end{aligned} \quad (52)$$

where $\mathcal{T}_\beta \mathbf{g} = \mathbf{g} \cdot \mathbf{n}|_{\partial\Omega_1}$ is the normal trace. For the subdomain with the Neumann boundary condition Ω_2 , seek $\mathbf{e}_\alpha \in H^1(\Omega_2)$ and $\mathbf{e}_\beta \in [L^2(\Omega_2)]^d$ to satisfy $\forall v_\alpha \in H^1(\Omega_2)$ and $\forall \mathbf{v}_\beta \in [L^2(\Omega_2)]^d$

$$\begin{aligned} (v_\alpha, \partial_t e_\alpha)_{\Omega_2} &= -(\text{grad } v_\alpha, \mathbf{e}_\beta)_{\Omega_2} + \langle \mathcal{T}_\alpha v_\alpha, u_{\partial,2} \rangle_{\Gamma_2} + \langle \mathcal{T}_\alpha v_\alpha, u_{\partial,2}^{\Gamma_{\text{int}}} \rangle_{\Gamma_{\text{int}}}, \\ (\mathbf{v}_\beta, \partial_t \mathbf{e}_\beta)_{\Omega_2} &= (\mathbf{v}_\beta, \text{grad } \mathbf{e}_\alpha)_{\Omega_2}, \end{aligned} \quad (53)$$

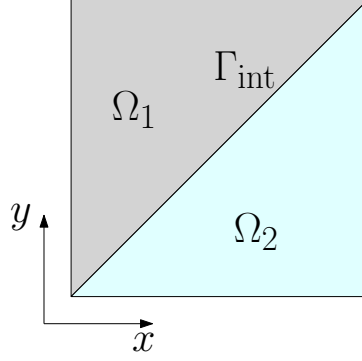


Figure 8: Domain splitting for the wave equation

where $\mathcal{T}_\alpha f = f|_{\partial\Omega_2}$ is the Dirichlet trace. The finite dimensional system for the Ω_1 subdomain becomes

$$\begin{aligned} \begin{bmatrix} \mathbf{M}_{\alpha,1} & 0 \\ 0 & \mathbf{M}_{\beta,1} \end{bmatrix} \frac{d}{dt} \begin{pmatrix} \mathbf{e}_{\alpha,1} \\ \mathbf{e}_{\beta,1} \end{pmatrix} &= \begin{bmatrix} 0 & \mathbf{D}_{\text{div}} \\ -\mathbf{D}_{\text{div}}^\top & 0 \end{bmatrix} \begin{pmatrix} \mathbf{e}_{\alpha,1} \\ \mathbf{e}_{\beta,1} \end{pmatrix} + \begin{bmatrix} 0 & 0 \\ \mathbf{B}_\beta^{\Gamma_1} & \mathbf{B}_\beta^{\Gamma_{\text{int}}} \end{bmatrix} \begin{pmatrix} \mathbf{u}_{\partial,1} \\ \mathbf{u}_{\partial,1}^{\text{int}} \end{pmatrix}, \\ \begin{pmatrix} \mathbf{y}_{\partial,1} \\ \mathbf{y}_{\partial,1}^{\text{int}} \end{pmatrix} &= \begin{bmatrix} 0 & \mathbf{T}_\beta^{\Gamma_1} \\ 0 & \mathbf{T}_\beta^{\Gamma_{\text{int}}} \end{bmatrix} \begin{pmatrix} \mathbf{e}_{\alpha,1} \\ \mathbf{e}_{\beta,1} \end{pmatrix}, \end{aligned} \quad (54)$$

while for the Ω_2 subdomain it becomes

$$\begin{aligned} \begin{bmatrix} \mathbf{M}_{\alpha,2} & 0 \\ 0 & \mathbf{M}_{\beta,2} \end{bmatrix} \frac{d}{dt} \begin{pmatrix} \mathbf{e}_{\alpha,2} \\ \mathbf{e}_{\beta,2} \end{pmatrix} &= \begin{bmatrix} 0 & -\mathbf{D}_{\text{grad}} \\ \mathbf{D}_{\text{grad}}^\top & 0 \end{bmatrix} \begin{pmatrix} \mathbf{e}_{\alpha,2} \\ \mathbf{e}_{\beta,2} \end{pmatrix} + \begin{bmatrix} \mathbf{B}_\alpha^{\Gamma_2} & \mathbf{B}_\alpha^{\Gamma_{\text{int}}} \\ 0 & 0 \end{bmatrix} \begin{pmatrix} \mathbf{u}_{\partial,2} \\ \mathbf{u}_{\partial,2}^{\text{int}} \end{pmatrix}, \\ \begin{pmatrix} \mathbf{y}_{\partial,2} \\ \mathbf{y}_{\partial,2}^{\text{int}} \end{pmatrix} &= \begin{bmatrix} \mathbf{T}_\alpha^{\Gamma_2} & 0 \\ \mathbf{T}_\alpha^{\Gamma_{\text{int}}} & 0 \end{bmatrix} \begin{pmatrix} \mathbf{e}_{\alpha,2} \\ \mathbf{e}_{\beta,2} \end{pmatrix}. \end{aligned} \quad (55)$$

Numerical experiments For this example we consider two different numerical analyses:

- A convergence study;
- A conservation properties study. In particular a curl free condition of the two subdomains and the power balance will be investigated.

The simulations take place on a unit square, decomposed by an interface placed diagonally between the lower left and upper right vertex as shown in Fig 8. An analytical solution has been used for the boundary inputs and the verification of the simulations. The exact solution consists of a temporal and spatial part given by

$$f(t) = 2 \sin(\sqrt{2}t) + 3 \cos(\sqrt{2}t), \quad (56)$$

$$g(x, y) = \cos(x) \sin(y). \quad (57)$$

The exact solutions are given as

$$\mathbf{e}_\alpha^{ex} = g \frac{df}{dt}, \quad \mathbf{e}_\beta^{ex} = f \text{grad } g, \quad (58)$$

The boundary conditions have been obtained from the exact solutions

$$e_\alpha|_{\Gamma_1} = g \frac{df}{dt}, \quad \mathbf{e}_\beta \cdot \mathbf{n}|_{\Gamma_2} = f \nabla_{\mathbf{n}} g|_{\Gamma_2},$$

where \mathbf{n} denotes the outward unit normal.

Finite element spaces The mesh consists of a structured triangular mesh. Discontinuous Galerkin or order $k-1$ and Raviart-Thomas or order k (RT_k) elements are used for $\mathbf{e}_{\alpha,1}$ and $\mathbf{e}_{\beta,1}$ respectively on the Ω_1 subdomain. Continuous Galerkin or order k (CG_k)

element for $e_{\alpha,2}$, the Nédélec first kind or order k (NED_k) for $e_{\beta,2}$ on the Ω_2 subdomain. The justification for this choice comes from de Rham complex and the subcomplex obtained using finite element differential forms of the trimmed polynomial family. The corresponding complex and subcomplex are given by

$$\begin{array}{ccc} H^{\text{div}} & \xrightarrow{\text{div}} & L^2 \\ \downarrow \Pi & & \downarrow \Pi \\ \text{RT}_k & \xrightarrow{\text{div}} & \text{DG}_{k-1} \end{array} \qquad \begin{array}{ccc} H^1 & \xrightarrow{\text{grad}} & H^{\text{curl}} \\ \downarrow \Pi & & \downarrow \Pi \\ \text{CG}_k & \xrightarrow{\text{grad}} & \text{NED}_k \end{array}$$

The solution is again found on union of meshes, that is $\mathfrak{T}_h = \mathfrak{T}_h^{\Omega_1} \cup \mathfrak{T}_h^{\Omega_2}$, with finite dimensional spaces for the Ω_1 subdomain given by

$$\begin{aligned} V_{\alpha,1} &= \{u_h \in L^2(\Omega_1) \mid \forall T \in \mathfrak{T}_h^{\Omega_1}, u_h|_T \in \text{DG}\}, \\ V_{\beta,1} &= \{\mathbf{u}_h \in H^{\text{div}}(\Omega_1) \mid \forall T \in \mathfrak{T}_h^{\Omega_1}, \mathbf{u}_h|_T \in \text{RT}\}, \end{aligned} \tag{59}$$

where T now denotes a triangular mesh element of \mathfrak{T}_h . For the Ω_2 subdomain the mixed finite element spaces are

$$\begin{aligned} V_{\alpha,2} &= \{u_h \in H^1(\Omega_2) \mid \forall T \in \mathfrak{T}_h^{\Omega_2}, u_h|_T \in \text{CG}\}, \\ V_{\beta,2} &= \{\mathbf{u}_h \in H^{\text{curl}}(\Omega_2) \mid \forall T \in \mathfrak{T}_h^{\Omega_2}, \mathbf{u}_h|_T \in \text{Ned}\}. \end{aligned} \tag{60}$$

Results The spatial convergence has been investigated by performing simulations for five different spatial step sizes h and three polynomial degrees for a total of 15 simulations. The results are shown in Figure 9 for the variables e_α and e_β for both the Ω_1 and Ω_2 subdomains. The theoretical convergence rates are denoted as h^k where k is the polynomial degree, e.g. $k = 1$ is the first polynomial degree. The rates of convergence for is observed to match well with the theoretical convergence rate h^k . The convergence of e_α on Ω_2 behaves slightly differently. For a polynomial order of $k = 1$, it converges with h^{k+1} , while for higher polynomial orders it converges with h^k . This is due to the fact that for Ω_2 it is discretized with a Lagrange element (whose convergence is given by h^{k+1} in the L^2 norm) whereas on Ω_1 it is discretized by a discontinuous Galerkin element (that converges with a rate h^k). The second equation in 53 is satisfied strongly because of the inclusion $V_{\beta,2} \subset \text{grad } V_{\alpha,2}$. This means that the following holds

$$\text{curl } \partial_t \mathbf{e}_\beta = \text{curl } \text{grad } e_\alpha = 0.$$

The curl free condition is instead only satisfied weakly in Eq. 52. Indeed, suppose $\mathbf{v}_\beta = \text{curl } \mathbf{v}$, where \mathbf{v} is chosen in a Nédélec space (recall that $\text{curl Ned}_k \subset \text{RT}_k$ so this is a valid choice of test function), then it holds that

$$(\text{curl } \mathbf{v}, \partial_t \mathbf{e}_\beta)_{\Omega_1} = (\text{div } \text{curl } \mathbf{v}, e_\alpha)_{\Omega_1} = 0,$$

for vanishing boundary conditions. The L^2 norm of $\text{curl } \mathbf{e}_\beta$ is plotted in Figure 10 and it is zero within machine precision. Since an implicit midpoint method is used to advance the solution of each domain, a power balance is satisfied for each system [20]. Since the solution for Ω_1 is computed at integer time steps, it holds

$$\frac{H_1^{n+1} - H_1^n}{\Delta t} - \langle \mathbf{y}_\partial^{n+\frac{1}{2}}, \mathbf{u}_\partial^{n+\frac{1}{2}} \rangle_{\partial\Omega_1} = 0.$$

For Ω_2 the solution is advanced at half-integer time steps so

$$\frac{H_2^{n+\frac{1}{2}} - H_2^{n-\frac{1}{2}}}{\Delta t} - \langle \mathbf{y}_\partial^{n+1}, \mathbf{u}_\partial^{n+1} \rangle_{\partial\Omega_2} = 0.$$

The power balance is determined for both the Ω_1 and Ω_2 subdomains in Figures 11. For both parts of the domain the power balance is observed to be in the order of 10^{-12} , hence zero within machine precision.

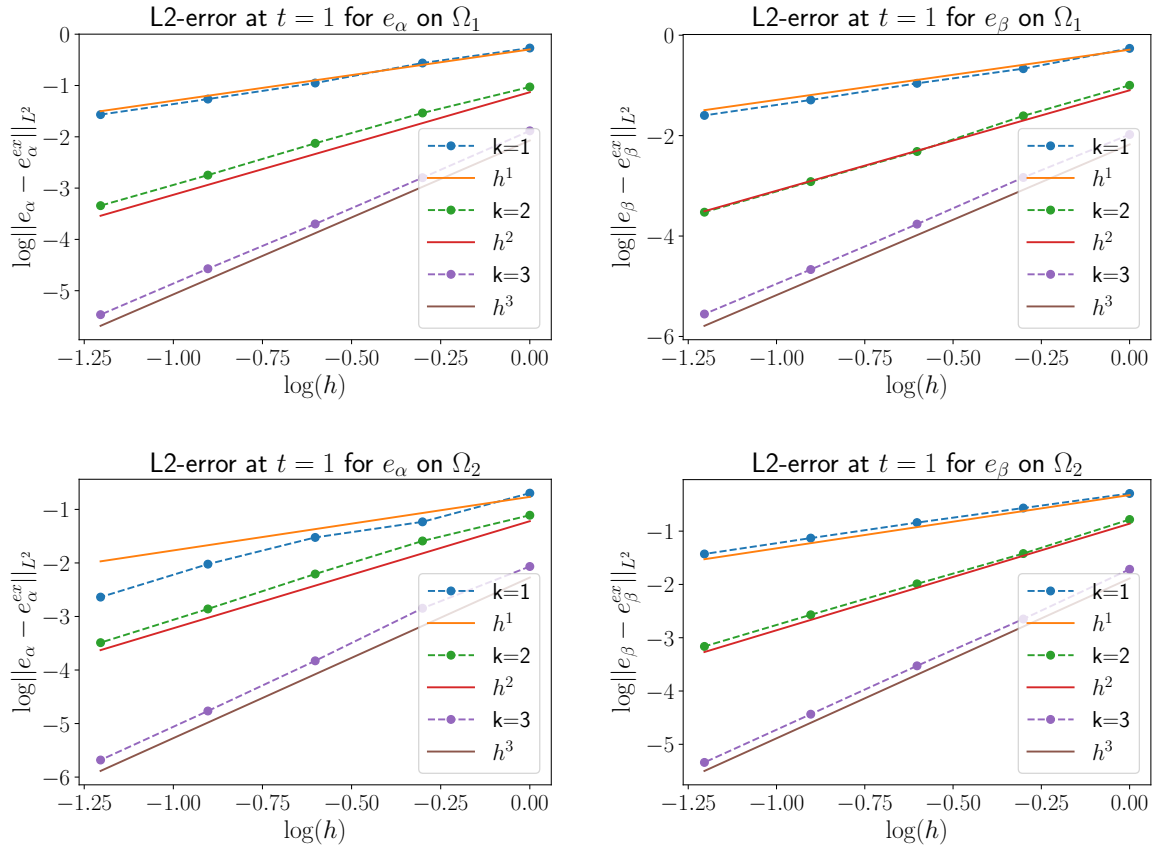


Figure 9: Convergence rates for wave equation compared with the expected convergences rates.

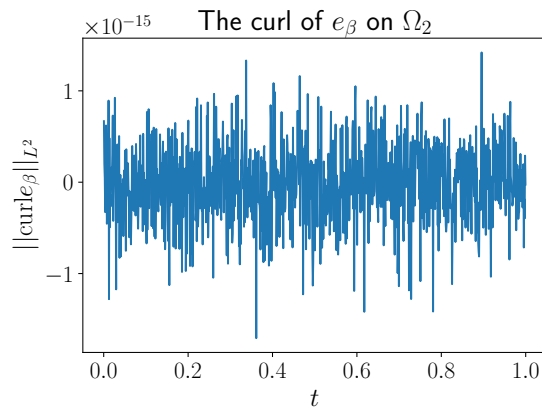


Figure 10: The value of $\text{curl} e_\beta$ on the Ω_2 subdomain.

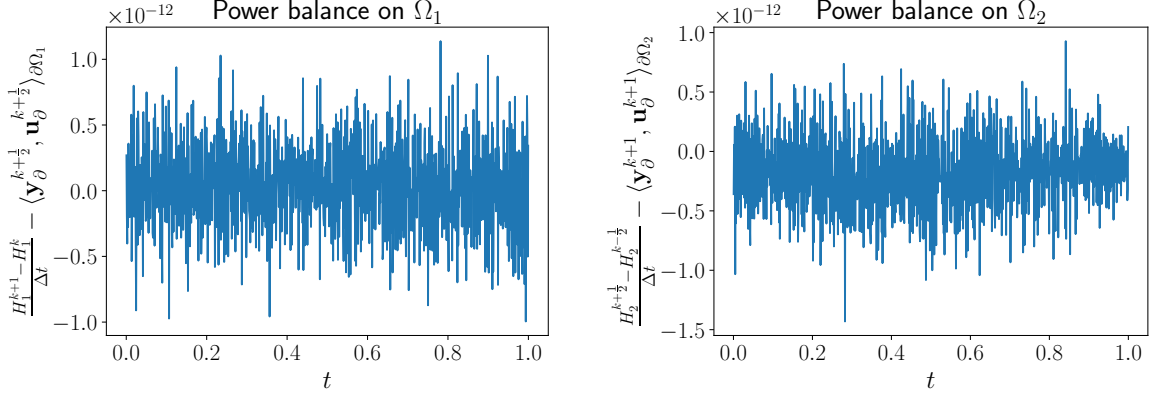


Figure 11: The power balance for the wave equation in two dimensions.

4.3 Maxwell Equations in 3D

The Maxwell equations on the unit cube $\Omega = [0, 1]^3$ are considered in this section

$$\begin{aligned} \epsilon \partial_t \mathbf{E} - \text{curl } \mathbf{H} &= 0, & \Omega &= [0, 1]^3, \\ \mu \partial_t \mathbf{H} + \text{curl } \mathbf{E} &= 0, \end{aligned} \quad (61)$$

where ϵ is the electric permittivity and μ the magnetic permeability. The Maxwell equations 61 can be expressed in terms of energy and co-energy variables as in 5

$$\begin{pmatrix} \epsilon \partial_t \mathbf{e}_\alpha \\ \mu \partial_t \mathbf{e}_\beta \end{pmatrix} = \begin{bmatrix} 0 & \text{curl} \\ -\text{curl} & 0 \end{bmatrix} \begin{pmatrix} \mathbf{e}_\alpha \\ \mathbf{e}_\beta \end{pmatrix}, \quad (62)$$

where the linear differential operator for the Maxwell equation is the $\mathcal{L} = -\text{curl}$ and likewise its formal adjoint $\mathcal{L}^* = -\text{curl}$. For the weak formulation on Ω_1 , based on 11, find $\mathbf{e}_\alpha \in H^{\text{curl}}(\Omega_1)$ and $\mathbf{e}_\beta \in [L^2(\Omega_1)]^3$ such that $\forall \mathbf{v}_\alpha \in [L^2(\Omega_1)]^3$ and $\forall \mathbf{v}_\beta \in H^{\text{curl}}(\Omega_1)$ it holds

$$\begin{aligned} (\mathbf{v}_\alpha, \epsilon \partial_t \mathbf{e}_\alpha)_{\Omega_1} &= -(\mathbf{v}_\alpha, \text{curl } \mathbf{e}_\beta)_{\Omega_1}, \\ (\mathbf{v}_\alpha, \mu \partial_t \mathbf{e}_\beta)_{\Omega_1} &= (\text{curl } \mathbf{v}_\beta, \mathbf{e}_\alpha)_{\Omega_1} + \langle \mathcal{T}_\beta \mathbf{v}_\beta, \mathbf{u}_{\partial, \alpha} \rangle_{\Gamma_1} + \langle \mathcal{T}_\beta \mathbf{v}_\beta, \mathbf{u}_{\partial, \alpha}^{\Gamma_{\text{int}}} \rangle_{\Gamma_{\text{int}}}, \end{aligned} \quad (63)$$

where the trace \mathcal{T}_β is given by

$$\mathcal{T}_\beta \mathbf{H} = \mathbf{H} \times \mathbf{n}|_{\Gamma_2}.$$

For the other subdomain Ω_2 the weak formulation is obtained by finding $\mathbf{e}_\alpha \in [L^2(\Omega_2)]^3$ and $\mathbf{e}_\beta \in H^{\text{curl}}(\Omega_2)$ to satisfy $\forall \mathbf{v}_\alpha \in H^{\text{curl}}(\Omega_2)$ and $\forall \mathbf{v}_\beta \in [L^2(\Omega_2)]^3$

$$\begin{aligned} (\mathbf{v}_\alpha, \epsilon \partial_t \mathbf{e}_\alpha)_{\Omega_2} &= -(\text{curl } \mathbf{v}_\alpha, \mathbf{e}_\beta)_{\Omega_2} + \langle \mathcal{T}_\alpha \mathbf{v}_\alpha, \mathbf{u}_{\partial, \beta} \rangle_{\Gamma_2} + \langle \mathcal{T}_\alpha \mathbf{v}_\alpha, \mathbf{u}_{\partial, \beta}^{\Gamma_{\text{int}}} \rangle_{\Gamma_{\text{int}}}, \\ (\mathbf{v}_\beta, \mu \partial_t \mathbf{e}_\beta)_{\Omega_2} &= (\mathbf{v}_\beta, \text{curl } \mathbf{v}_\alpha)_{\Omega_2}, \end{aligned} \quad (64)$$

where the trace \mathcal{T}_α is given by

$$\mathcal{T}_\alpha \mathbf{E} = (\mathbf{E} \times \mathbf{n}) \times \mathbf{n}|_{\Gamma_1}.$$

Based on the case described by 12. The system of equations can then be written as in 31

$$\begin{aligned} \begin{bmatrix} \mathbf{M}_{\alpha,1} & 0 \\ 0 & \mathbf{M}_{\beta,1} \end{bmatrix} \frac{d}{dt} \begin{pmatrix} \mathbf{e}_{\alpha,1} \\ \mathbf{e}_{\alpha,1} \end{pmatrix} &= \begin{bmatrix} 0 & \mathbf{D}_{\text{curl}} \\ -\mathbf{D}_{\text{curl}}^\top & 0 \end{bmatrix} \begin{pmatrix} \mathbf{e}_{\alpha,1} \\ \mathbf{e}_{\alpha,1} \end{pmatrix} + \begin{bmatrix} 0 & 0 \\ \mathbf{B}_\beta^{\Gamma_1} & \mathbf{B}_\beta^{\Gamma_{\text{int}}} \end{bmatrix} \begin{pmatrix} \mathbf{u}_{\partial,1} \\ \mathbf{u}_{\partial,1}^{\text{int}} \end{pmatrix}, \\ \begin{pmatrix} \mathbf{y}_{\partial,1} \\ \mathbf{y}_{\partial,1}^{\text{int}} \end{pmatrix} &= \begin{bmatrix} 0 & \mathbf{T}_\beta^{\Gamma_1} \\ 0 & \mathbf{T}_\beta^{\Gamma_{\text{int}}} \end{bmatrix} \begin{pmatrix} \mathbf{e}_{\alpha,1} \\ \mathbf{e}_{\alpha,1} \end{pmatrix}, \end{aligned} \quad (65)$$

for the Ω_1 subdomain. For Ω_2 the system of inputs and outputs is given by 32 as

$$\begin{aligned} \begin{bmatrix} \mathbf{M}_{\alpha,2} & 0 \\ 0 & \mathbf{M}_{\beta,2} \end{bmatrix} \frac{d}{dt} \begin{pmatrix} \mathbf{e}_{\alpha,2} \\ \mathbf{e}_{\alpha,2} \end{pmatrix} &= \begin{bmatrix} 0 & \mathbf{D}_{\text{curl}}^\top \\ -\mathbf{D}_{\text{curl}} & 0 \end{bmatrix} \begin{pmatrix} \mathbf{e}_{\alpha,2} \\ \mathbf{e}_{\alpha,2} \end{pmatrix} + \begin{bmatrix} \mathbf{B}_\alpha^{\Gamma_2} & \mathbf{B}_\alpha^{\Gamma_{\text{int}}} \\ 0 & 0 \end{bmatrix} \begin{pmatrix} \mathbf{u}_{\partial,2} \\ \mathbf{u}_{\partial,2}^{\text{int}} \end{pmatrix}, \\ \begin{pmatrix} \mathbf{y}_{\partial,2} \\ \mathbf{y}_{\partial,2}^{\text{int}} \end{pmatrix} &= \begin{bmatrix} \mathbf{T}_\alpha^{\Gamma_2} & 0 \\ \mathbf{T}_\alpha^{\Gamma_{\text{int}}} & 0 \end{bmatrix} \begin{pmatrix} \mathbf{e}_{\alpha,2} \\ \mathbf{e}_{\alpha,2} \end{pmatrix}. \end{aligned} \quad (66)$$

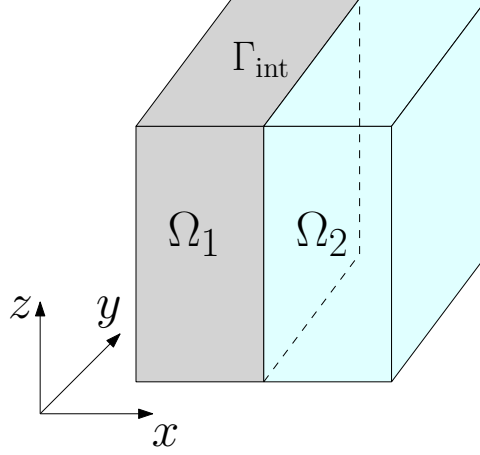


Figure 12: Domain decomposition for the Maxwell equations

Numerical experiments To verify the domain decomposition approach for the three dimensional Maxwell equations, the solenoidal nature of the electric and magnetic fields is verified and the discrete power balance of the domain decomposition discretization is examined. The domain is divided by an interface surface Γ_{int} into

$$\Omega_1 = [0, 1/2] \times [0, 1] \times [0, 1], \quad \Omega_2 = [1/2, 1] \times [0, 1] \times [0, 1],$$

as shown in Figure 12. An exact eigen-solution is used to test the scheme. The spatial and temporal functions are given by

$$\mathbf{g}(x, y, z) = \begin{pmatrix} -\cos(x) \sin(y) \sin(z) \\ 0 \\ \sin(x) \sin(y) \cos(z) \end{pmatrix}, \quad f(t) = \frac{\sin(\omega t)}{\omega}, \quad (67)$$

where $\omega = \sqrt{\frac{3}{\epsilon\mu}}$. The exact solution is then written as follows

$$\mathbf{e}_\alpha^{ex} = \mu \mathbf{g} \frac{df}{dt}, \quad \mathbf{e}_\beta^{ex} = -\text{curl}(\mathbf{g})f \quad (68)$$

Finite element spaces The mesh consists of as structured tetrahedral elements. Raviart-Thomas (RT_k) elements and Nédélec (NED_k) elements of order k are used for $e_{\alpha,1}$ and $e_{\beta,1}$ respectively on the Ω_1 subdomain. Nédélec elements for $e_{\alpha,2}$ and Raviart-Thomas for $e_{\beta,2}$ are instead used on the Ω_2 subdomain. This choice follows from the following Hilbert complex

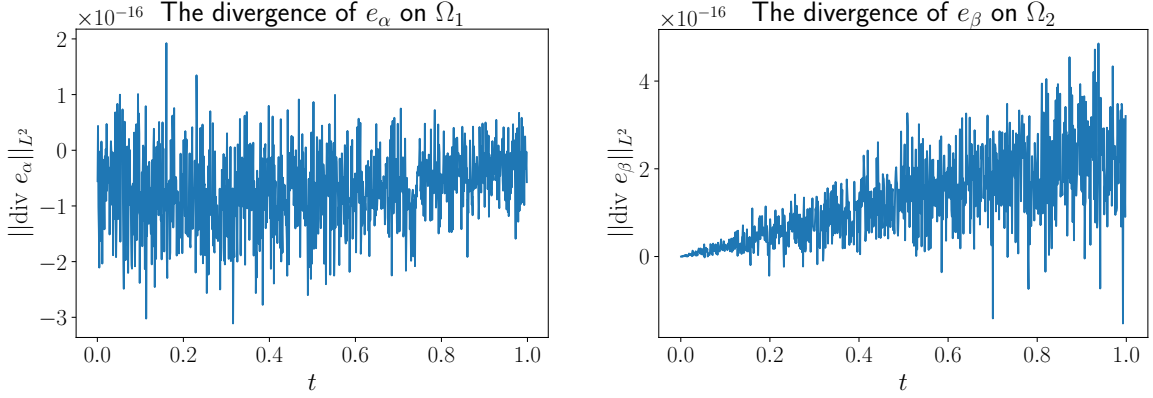
$$\begin{array}{ccc} H^{\text{curl}} & \xrightarrow{\text{curl}} & H^{\text{div}} \\ \downarrow \Pi & & \downarrow \Pi \\ \text{NED}_k & \xrightarrow{\text{curl}} & \text{RT}_k \end{array}$$

The spaces for the Ω_1 subdomain are given by

$$\begin{aligned} V_{\alpha,1} &= \{\mathbf{u}_h \in H^{\text{div}}(\Omega_2) | \forall T \in \mathcal{T}_h^{\Omega_2}, \mathbf{u}_h|_T \in \text{RT}_k\}, \\ V_{\beta,1} &= \{\mathbf{u}_h \in H^{\text{curl}}(\Omega_2) | \forall T \in \mathcal{T}_h^{\Omega_2}, \mathbf{u}_h|_T \in \text{Ned}_k\}, \end{aligned} \quad (69)$$

whereas for the Ω_2 domain the mixed finite elements spaces are

$$\begin{aligned} V_{\alpha,2} &= \{\mathbf{u}_h \in H^{\text{curl}}(\Omega_1) | \forall T \in \mathcal{T}_h^{\Omega_1}, \mathbf{u}_h|_T \in \text{Ned}_k\}, \\ V_{\beta,1} &= \{\mathbf{u}_h \in H^{\text{div}}(\Omega_1) | \forall T \in \mathcal{T}_h^{\Omega_1}, \mathbf{u}_h|_T \in \text{RT}_k\}. \end{aligned} \quad (70)$$



(a) The $\text{div } e_\alpha$ on Ω_1 .

(b) The $\text{div } e_\beta$ on Ω_2 .

Figure 13: The divergence on the different subdomains.

Results For the numerical simulation, the following values of the electric permittivity and magnetic permeability are considered

$$\epsilon = 2, \quad \mu = \frac{3}{2}$$

The first equation in 63 is verified strongly by the discrete formulation

$$\mu \partial_t \text{div } \mathbf{e}_\alpha = -\text{div curl } \mathbf{e}_\beta = 0.$$

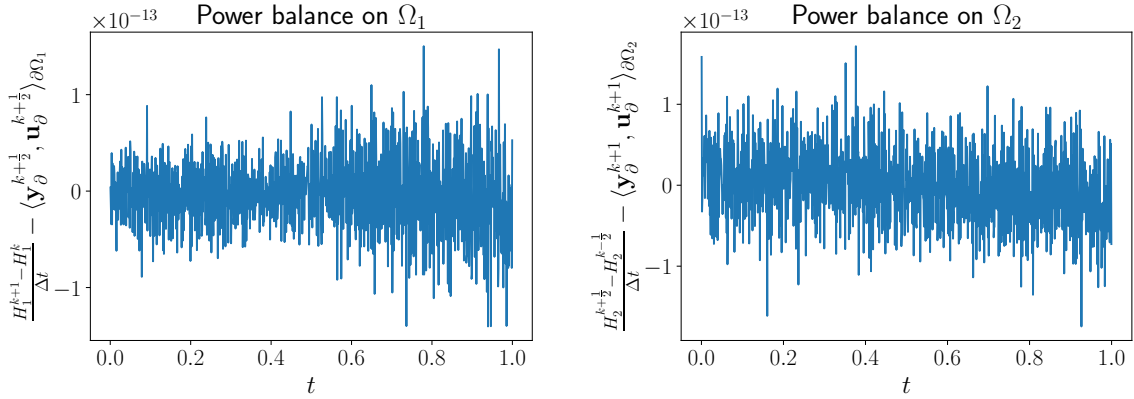
This equations states that the electrical field is solenoidal in the absence of electrical charges. The second equation in 64

$$\epsilon \partial_t \text{div } \mathbf{e}_\beta = \text{div curl } \mathbf{e}_\alpha = 0,$$

states instead that the magnetic field is solenoidal and is strongly satisfied by the formulation. From these relation the divergence of \mathbf{e}_α and \mathbf{e}_β should be zero on the subdomains Ω_1 and Ω_2 respectively. Meanwhile, the divergence of \mathbf{e}_β and \mathbf{e}_α are weakly enforced on Ω_1 and Ω_2 respectively, and are therefore not expected to be zero in their respective subdomains. The results are shown in Figure 13. As predicted, it holds $\text{div } \mathbf{e}_\alpha = 0$ on Ω_1 and $\text{div } \mathbf{e}_\beta = 0$ on Ω_2 are in the order of 10^{-16} , thus they are zero within machine precision regardless of the coarseness of the mesh. The discretization with domain decomposition is able to preserve the divergence free condition on the discrete level for \mathbf{e}_α on the Ω_1 subdomain, and for \mathbf{e}_β on the Ω_2 subdomain. According to the discretization the power balance should be preserved exactly. The power balance for the two subdomains have been plotted in Figure 14, and is indeed observed the be preserved within machine precision for the Maxwell equations in three dimensions.

5 Conclusion

In this contribution, a numerical scheme to imposed mixed boundary conditions naturally was derived by decomposing the domain into subdomains with homogeneous boundary conditions. Two different weak formulation with opposite causalities are considered on each subdomain. The methodology is based on the concept of Hilbert subcomplex and the underlying mathematical framework. To verify that the proposed discretization is able to transfer information across the interface without loss of accuracy or capability to preserve mathematical structures, it has been applied to three different test cases. The one dimensional Euler-Bernoulli beam, the two dimensional wave equation and lastly the Maxwell equation in three dimensions. It results showed that the proposed approach is able to attain accurate results with good convergence. In addition it exactly preserves the discrete power balance, as was shown for the wave and Maxwell equations. Structures such as the curl free condition present in the wave equation was observed to be within machine precision in



(a) Power balance for the Ω_1 subdomain.

(b) Power balance for the Ω_2 subdomain.

Figure 14: The power balance for the three dimensional Maxwell equations using dual field domain decomposition.

part of the domain. In the Maxwell equation the electric and magnetic fields satisfy the divergence free condition for the electric and magnetic field, albeit on different domains.

The proposed formulation requires the definition of an interface between two subdomain. This may represent a bottleneck in applications where the boundary subpartitions present an intricate topology. However, this contribution represents a proof of concept of using simultaneously two mixed formulations. This strategy allows to treat problems with mixed boundary conditions as ordinary differential equations rather than differential algebraic equations (that are notoriously more difficult to treat numerically). A natural extension of the proposed methodology would be to push the idea further and consider a discontinuous Galerkin framework where the fluxes on the primal system are obtained using the dual system and vice-versa. The presented idea may also find application in static problems, very much in the same spirit of hybrid and discontinuous methods.

Funding

This research was carried out under project number N21006 in the framework of the Partnership Program of the Material innovation institute M2i (www.m2i.nl) and the Dutch Research Council (www.nwo.nl). This work was supported by the PortWings project funded by the European Research Council [Grant Agreement No. 787675].

Acknowledgements

The second author would like to thank Flavio Cardoso Ribeiro (Technical Institute of Aeronautics) and Paul Kotyczka (Technical University of Munich) for fruitful discussions on this topic.

References

- [1] V. Duindam, A. Macchelli, S. Stramigioli, H. Bruyninckx, Modeling and control of complex physical systems: the port-Hamiltonian approach, Springer Science & Business Media, Berlin Heidelberg, 2009.
- [2] P. Bochev, A discourse on variational and geometric aspects of stability of discretizations, 33rd Computational Fluid Dynamics Lecture Series, VKI LS 5 (2003).
- [3] D. N. Arnold, R. S. Falk, R. Winther, Finite element exterior calculus, homological techniques, and applications, Acta numerica 15 (2006) 1–155.

- [4] S. H. Christiansen, H. Z. Munthe-Kaas, B. Owren, Topics in structure-preserving discretization, *Acta Numerica* 20 (2011) 1–119. doi:10.1017/S096249291100002X.
- [5] P. B. Bochev, J. M. Hyman, Principles of mimetic discretizations of differential operators, in: *Compatible spatial discretizations*, Springer, 2006, pp. 89–119.
- [6] K. Lipnikov, G. Manzini, M. Shashkov, Mimetic finite difference method, *Journal of Computational Physics* 257 (2014) 1163–1227, physics-compatible numerical methods. doi:10.1016/j.jcp.2013.07.031.
- [7] A. N. Hirani, Discrete exterior calculus, Ph.D. thesis, California Institute of Technology, Pasadena, CA (2003).
- [8] A. van der Schaft, B. Maschke, Hamiltonian formulation of distributed-parameter systems with boundary energy flow, *Journal of Geometry and Physics* 42 (1) (2002) 166–194. doi:10.1016/S0393-0440(01)00083-3.
- [9] A. Quarteroni, A. Valli, Numerical approximation of partial differential equations, Vol. 23, Springer Science & Business Media, Berlin, Heidelberg, 2008.
- [10] Y. Bazilevs, T. Hughes, Weak imposition of dirichlet boundary conditions in fluid mechanics, *Computers & Fluids* 36 (1) (2007) 12–26, challenges and Advances in Flow Simulation and Modeling. doi:10.1016/j.compfluid.2005.07.012.
- [11] G. Eriksson, K. Mattsson, Weak versus strong wall boundary conditions for the incompressible Navier-Stokes equations, *Journal of Scientific Computing* 92 (3) (2022) 81. doi:10.1007/s10915-022-01941-5.
- [12] P. Kunkel, V. Mehrmann, Differential-algebraic equations: analysis and numerical solution, Vol. 2, European Mathematical Society, Zürich, 2006.
- [13] M. Seslija, J. M. Scherpen, A. van der Schaft, Explicit simplicial discretization of distributed-parameter port-Hamiltonian systems, *Automatica* 50 (2) (2014) 369–377. doi:10.1016/j.automatica.2013.11.020.
- [14] P. Kotyczka, B. Maschke, L. Lefèvre, Weak form of Stokes–Dirac structures and geometric discretization of port-Hamiltonian systems, *Journal of Computational Physics* 361 (2018) 442–476. doi:10.1016/j.jcp.2018.02.006.
- [15] F. L. Cardoso-Ribeiro, D. Matignon, L. Lefèvre, A partitioned finite element method for power-preserving discretization of open systems of conservation laws, *IMA Journal of Mathematical Control and Information* 38 (2) (2020) 493–533. doi:10.1093/imamci/dnaa038.
- [16] N. Kumar, J. J. W. van der Vegt, H. J. Zwart, Port-hamiltonian discontinuous galerkin finite element methods, *IMA Journal of Numerical Analysis* (2024) drae008doi:10.1093/imanum/drae008.
- [17] P. Joly, Variational Methods for Time-Dependent Wave Propagation Problems, Springer Berlin Heidelberg, Berlin, Heidelberg, 2003, pp. 201–264. doi:10.1007/978-3-642-55483-4_6.
- [18] A. Brugnoli, R. Rashad, S. Stramigioli, Dual field structure-preserving discretization of port-Hamiltonian systems using finite element exterior calculus, *Journal of Computational Physics* 471 (12 2022). doi:10.1016/j.jcp.2022.111601.
- [19] Y. Zhang, A. Palha, M. Gerritsma, L. G. Rebholz, A mass-, kinetic energy- and helicity-conserving mimetic dual-field discretization for three-dimensional incompressible Navier-Stokes equations, part I: Periodic domains, *Journal of Computational Physics* 451 (2 2022). doi:10.1016/j.jcp.2021.110868.
- [20] P. Kotyczka, L. Lefèvre, Discrete-time port-Hamiltonian systems: A definition based on symplectic integration, *Systems & Control Letters* 133 (2019) 104530. doi:10.1016/j.sysconle.2019.104530.
- [21] J. E. Marsden, T. S. Ratiu, Introduction to Mechanics and Symmetry: A Basic Exposition of Classical Mechanical Systems, 2nd Edition, Texts in Applied Mathematics, Springer, New York, NY, 1999. doi:10.1007/978-0-387-21792-5.
- [22] A. Brugnoli, V. Mehrmann, On the discrete equivalence of Lagrangian, Hamiltonian and mixed finite element formulations for linear wave phenomena, *IFAC-PapersOnLine* 58 (6) (2024) 95–100. doi:10.1016/j.ifacol.2024.08.263.

- [23] J. M. Sanz-Serna, Symplectic integrators for Hamiltonian problems: An overview, *Acta Numerica* 1 (1992) 243–286. doi:10.1017/S0962492900002282.
- [24] C. Geuzaine, J.-F. Remacle, Gmsh: A 3-D finite element mesh generator with built-in pre- and post-processing facilities, *International Journal for Numerical Methods in Engineering* 79 (11) (2009) 1309–1331. doi:10.1002/nme.2579.
- [25] F. Rathgeber, D. A. Ham, L. Mitchell, M. Lange, F. Luporini, A. T. McRae, G. T. Bercea, G. R. Markall, P. H. Kelly, Firedrake: Automating the finite element method by composing abstractions, *ACM Transactions on Mathematical Software* 43 (3) (12 2016). doi:10.1145/2998441.
- [26] M. Krstic, A. Smyshlyaev, *Boundary Control of PDEs*, Society for Industrial and Applied Mathematics, Philadelphia, PA, 2008. doi:10.1137/1.9780898718607.
- [27] F. Bonizzoni, K. Hu, G. Kanschat, D. Sap, Discrete tensor product BGG sequences: splines and finite elements, *Mathematics of Computation* (2024).